Semiquantal molecular dynamics simulations of hydrogen-bond dynamics in liquid water using multi-dimensional Gaussian wave packets

Junichi Ono and Koji Ando

Additional information on J. Chem. Phys.

Semiquantal molecular dynamics simulations of hydrogen-bond dynamics in liquid water using multi-dimensional Gaussian wave packets

Junichi Ono[a] and Koji Ando

Department of Chemistry, Graduate School of Science, Kyoto University, Kyoto 606-8502, Japan

A semiquantal (SQ) molecular dynamics (MD) simulation method based on an extended Hamiltonian formulation has been developed using multi-dimensional thawed Gaussian wave packets (WPs), and applied to an analysis of hydrogen-bond (H-bond) dynamics in liquid water. A set of Hamilton's equations of motion in an extended phase space, which includes variance-covariance matrix elements as auxiliary coordinates representing anisotropic delocalization of the WPs, is derived from the time-dependent variational principle. The present theory allows us to perform real-time and real-space SQMD simulations and analyze nuclear quantum effects on dynamics in large molecular systems in terms of anisotropic fluctuations of the WPs. Introducing the Liouville operator formalism in the extended phase space, we have also developed an explicit symplectic algorithm for the numerical integration, which can provide greater stability in the long-time SQMD simulations. The application of the present theory to H-bond dynamics in liquid water is carried out under a single-particle approximation in which the variance-covariance matrix and the corresponding canonically conjugate matrix are reduced to block-diagonal structures by neglecting the interparticle correlations. As a result, it is found that the anisotropy of the WPs is indispensable for reproducing the disordered H-bond network compared to the classical counterpart with the use of the potential model providing competing quantum effects between intra- and intermolecular zero-point fluctuations. In addition, the significant WP delocalization along the out-of-plane direction of the jumping hydrogen atom associated with the concerted breaking and forming of H-bonds has been detected in the H-bond exchange mechanism. The relevance of the dynamical WP broadening to the relaxation of H-bond number fluctuations has also been discussed. The present SQ method provides the novel framework for investigating nuclear quantum dynamics in the many-body molecular systems in which the local anisotropic fluctuations of nuclear WPs play an essential role. © *2012 American Institute of Physics.* [http://dx.doi.org/10.1063/1.4762840]

I. INTRODUCTION

It has been recognized that the three-dimensional (3D) hydrogen-bond (H-bond) network formed by water molecules plays a fundamental role in varied chemical and biological processes,[1–8] and extensive theoretical and experimental efforts have been devoted to elucidating its mechanism to date.[9–24] The 3D H-bond network is also responsible for well-known peculiar properties of water such as density maximum at $4.0\,°C$ and high melting temperature $(0.0\,°C)$.[1] In these properties, nuclear quantum effects are found to be significant; for instance, the densities of deuterated water (D_2O) and tritiated water (T_2O) become maximum at $11.2\,°C$ and $13.4\,°C$, respectively.[1] The isotopic differences are also notable in the melting points: $3.8\,°C$ and $4.5\,°C$ for D_2O and T_2O, respectively.[25] These observations indicate that nuclear quantum fluctuations of the hydrogen atoms have a strong influence on energy and structure of the 3D H-bond network and then result in the significant isotope effects on macroscopic properties of water. Although the physical origin of these quantum effects has long been interpreted as zero-point energy,[26] a molecular-level description of nuclear quantum fluctuations in terms of dynamical proton delocalization and its relevance to reorganization dynamics of the H-bond network still remains elusive.

Developing the theoretical framework for the accurate description of real-time quantum dynamics in condensed phases remains one of the most challenging problems in physics and chemistry. Although the exact thermodynamic and structural properties in many-body molecular systems can be practically obtained from imaginary-time path-integral (PI) simulations,[26–33] the exact calculation of quantum dynamical properties is still limited to small systems with a few degrees of freedom coupled to a simple bath.[34,35] Instead, classical molecular dynamics (MD) simulations are widely employed in order to investigate dynamical quantities from a microscopic perspective in large molecular systems with thousands of degrees of freedom.[36] However, nuclear quantum effects such as zero-point energy and delocalization of wave packets (WPs), which are indispensable for the accurate description of the dynamical fluctuations of light particles, are neglected in the usual classical MD simulations. Thus, there has been considerable interest in the development of computationally manageable approximation schemes for calculating quantum dynamical properties, and a number of different methods have been proposed; for example, the centroid MD

---
a)Electronic mail: ono@kuchem.kyoto-u.ac.jp.

137, 174503-1

method,[37–40] the ring polymer MD (RPMD) method,[41–44] and the linearized semiclassical initial value representation (LSC-IVR)[45–47] were developed as approximation schemes for computing quantum mechanical real-time correlation functions and applied to liquid water.[38–40,42–44,46,47]

The Gaussian WPs (GWPs) are useful tools for describing the approximate real-time quantum dynamics of nuclear WPs; for instance, the thawed GWPs[48,49] can directly capture the dynamical delocalization of quantum particles and provide the intuitive mechanism of the dynamical fluctuations of WPs, whereas the frozen GWPs are suitable as a basis set for quantum propagation.[50,51] In particular, the approximation schemes based on the multi-dimensional thawed GWPs for the real-time WP dynamics were derived from the local harmonic approximation[48] and the variational principle.[49,52–54] The thawed GWPs were also exploited in the multi-configuration time-dependent Hartree schemes[55–57] which are now extending applicability to large systems.[58] Furthermore, these ideas were recently extended to the imaginary-time GWP dynamics for efficient calculation of quantum static properties in clusters.[59,60] In these methods, however, the resulting equations of motion (EOMs) for some of the time-dependent Gaussian parameters (i.e., the width parameters) are not canonical form, and thus the time evolution of these variables is described in non-Hamiltonian dynamical systems in which symplectic structures[33,61,62] are absent.

Based on the time-dependent variational principle (TDVP),[63–66] the semiquantal (SQ) GWP methods within the framework of the Hamiltonian formulation were developed in a variety of forms mostly in the field of nuclear physics,[67–71] and applied to chemical problems with the time-dependent Hartree (TDH) ansatz of the squeezed coherent state functions.[72–76] In the SQGWP schemes, the real-time quantum dynamics in the Hilbert space is approximately replaced by the classical Hamiltonian dynamics in the extended phase space which includes auxiliary coordinates and momenta representing the WP widths.[72] The resulting extended Hamiltonian has a simple separable form, and thus the intuitive interpretation of the WP dynamics based upon the potential concept in the extended phase space can be provided.[72] Interestingly, the SQGWP theory is closely related to the second-order quantized Hamilton dynamics (QHD-2),[77–80] and is essentially equivalent to the second-order quantal cumulant dynamics (QCD-2).[81–84] It is also intriguing to note that the SQGWP framework has recently been extended to describe many electron systems[85,86] and electron-nuclear systems in the non-Born-Oppenheimer framework.[87]

Although the SQMD simulation method with the TDH ansatz can treat large molecular systems, the rotational invariance of WPs should be retained within the Hartree approximation.[88] Indeed, the spherically symmetric constraints[67] were adopted in the previous works,[71,74–76] in which the GWP of each of the quantum particles is restricted to the spherically symmetric structure at any time. However, the spherically symmetric assumption is apparently invalid in molecular systems such as water where the local directional interactions play an important role; in liquid water, for example, the molecules form the distorted tetrahedral H-bond network which continuously fluctuates,[4,5,7,8] and thus it is rea-sonable to suppose that the nuclear WPs form the anisotropic structure due to the local 3D interactions. Hence, it is desirable to extend the SQGWP theory without the spherically symmetric constraints in order to describe the anisotropic fluctuations of WPs with the rotational invariance.

The purposes of the present study are (i) to develop the SQGWP theory in a form suitable for general anisotropic systems, (ii) to formulate an explicit symplectic algorithm for robust time propagations by exploiting the canonical Hamiltonian form of the theory, and (iii) to implement the SQMD simulation of liquid water and examine the molecular jump mechanism of H-bond exchange dynamics.

First, we develop the theory along the previously suggested line,[89] or generalize the previous SQGWP theory using the correlated multi-dimensional thawed GWPs within the framework of the Hamiltonian formulation; in addition to the center coordinates of WPs and the conjugate momenta, the variance-covariance matrix and the corresponding conjugate matrix of the GWPs are introduced as the additional dynamical variables, so that it becomes possible to describe the anisotropic dynamical delocalization of WPs with the rotational invariance. We can then derive a set of Hamilton's EOMs in the extended phase space on the basis of the TDVP. As a result, the present theory enables us to carry out the real-time and real-space SQMD simulations in the extended phase space without the spherically symmetric constraints and to analyze the nuclear quantum dynamics in molecular systems in terms of the anisotropic fluctuations of WPs.

Second, we develop the explicit symplectic algorithm with the time reversibility for the numerical integration in the SQMD simulations based on the Liouville operator formalism in the extended phase space. The presence of symplectic algorithm, which can provide the long-time stability of trajectories, is one of the advantages of the Hamiltonian formulation.[61,62,90–93] However, the development of explicit symplectic algorithm in the present theory is not trivial since the resulting extended Hamiltonian is inevitably non-separable[70] due to the existence of the off-diagonal elements in the matrices. Here, we derive the time-reversible explicit symplectic algorithm using the symmetric Trotter theorem[33,94] and discuss the conserved Hamiltonian in the second-order symplectic algorithm in detail (see also Appendix B).

Third, we construct a practical approximation, which will be referred to as the single-particle approximation, in order to reduce the number of degrees of freedom which is proportional to the square of the system size.[52,54,59,60] In the single-particle approximation, the variance-covariance matrix and the corresponding conjugate matrix are reduced to block-diagonal structures by only considering correlations between the different degrees of freedom in one particle and neglecting the interparticle correlations. As a result, the number of degrees of freedom scales linearly with the system size and the computational costs of the matrix operations are significantly reduced.

The present paper is organized as follows. After brief discussion on the previous SQMD implementations with the TDH ansatz, the generalization into the correlated multi-dimensional GWP dynamics within the framework of the

Hamiltonian formulation is provided in Sec. II. Approximation schemes for evaluating the potential expectation are also given in this section. In Sec. III, the explicit symplectic algorithm with the time reversibility for the numerical integration in the current SQMD simulations is presented. In Sec. IV, the single-particle approximation based upon the single-particle ansatz is introduced, and then the simulation procedures are outlined. In Sec. V, discussion on the present results of liquid water is described. The paper finally concludes in Sec. VI.

II. GENERALIZED SEMIQUANTAL TIME-DEPENDENT THEORY

A. Correlated multi-dimensional Gaussian wave packet dynamics: Hamiltonian formulation

The implementation of the SQGWP theory for 3D many-body systems has previously been provided using two kinds of trial wave functions: a Hartree product of uncorrelated 3D GWPs[74] and that of spherically symmetric 3D GWPs.[74–76] Note that the rotational invariance of the WPs is broken under the former approximation since the WP width variables of each of the quantum particles are allowed to independently fluctuate only along the coordinate axes fixed in a simulation box. For this reason, all the previous applications were in fact carried out using the latter approximation in which the spherically symmetric constraints are imposed upon the 3D GWPs.[74–76]

Here, we discuss the generalization for a 3D many-body system within the framework of the Hamiltonian formulation. Consider the system consisting of N distinguishable particles described by the Hamiltonian

$$H = \sum_{j=1}^{N} \frac{|\mathbf{p}_j|^2}{2m_j} + V(\mathbf{q}_1, \ldots, \mathbf{q}_N), \tag{1}$$

where m_j, $\mathbf{q}_j \equiv (q_{jx}, q_{jy}, q_{jz})$, and $\mathbf{p}_j \equiv (p_{jx}, p_{jy}, p_{jz})$ denote the mass, the 3D Cartesian position vector, and the corresponding conjugate momentum vector of the jth quantum particle, respectively, and V is the (Born-Oppenheimer) potential function of the system. In the present study, we assume the trial wave function of the system to be a correlated multi-dimensional thawed Gaussian function[89] as

$$\Psi(\mathbf{q}, t) = (2\pi)^{-3N/4} \{\det(\mathbf{G})\}^{-1/4}$$
$$\times \exp\left[\Delta\mathbf{q}^{\mathrm{T}}\mathbf{A}\Delta\mathbf{q} + \frac{i}{\hbar}\mathbf{p}_r^{\mathrm{T}}\Delta\mathbf{q}\right], \tag{2}$$

where $\Delta\mathbf{q} \equiv (\mathbf{q} - \mathbf{r})$ describes the $3N$-dimensional displacement vector, $\mathbf{q} \equiv (\mathbf{q}_1, \ldots, \mathbf{q}_N)$ represents the $3N$-dimensional Cartesian position vector of the system, and $\mathbf{A}$ is the $3N \times 3N$ complex symmetric matrix defined by

$$\mathbf{A} = -\frac{1}{4}\mathbf{G}^{-1} + \frac{i}{\hbar}\mathbf{K}. \tag{3}$$

This function is specified by the time-dependent variational parameters: the $3N$-dimensional real vectors $\mathbf{r} \equiv (\mathbf{r}_1, \ldots, \mathbf{r}_N)$ and $\mathbf{p}_r \equiv (\mathbf{p}_{r_1}, \ldots, \mathbf{p}_{r_N})$, and the $3N \times 3N$ real symmetric matrices $\mathbf{G}$ and $\mathbf{K}$. Here, the number of independent degrees of freedom in each of the matrices is equal to $3N(3N + 1)/2$. Note that the matrix $\mathbf{G}$ is also positive definite. Then, the

physical meaning of these parameters can be seen from the following relations:

$$\langle q_{j\mu} \rangle = r_{j\mu}, \tag{4}$$

$$\langle p_{j\mu} \rangle = p_{r_{j\mu}}, \tag{5}$$

$$\langle \Delta q_{j\mu} \Delta q_{k\nu} \rangle = G_{j\mu, k\nu}, \tag{6}$$

$$\langle \Delta p_{j\mu} \Delta p_{k\nu} \rangle = \frac{\hbar^2}{4}(\mathbf{G}^{-1})_{j\mu, k\nu} + 4(\mathbf{KGK})_{j\mu, k\nu}, \tag{7}$$

$$\langle (\Delta q_{j\mu} \Delta p_{k\nu})_{\mathrm{s}} \rangle = 2(\mathbf{KG})_{j\mu, k\nu}, \tag{8}$$

where $\langle \ldots \rangle$ indicates the quantum mechanical expectation value defined by the trial function in Eq. (2), μ labels the spatial Cartesian components (i.e., $\mu = \{x, y, z\}$), and $(\ldots)_{\mathrm{s}}$ denotes a symmetrized product; i.e., $(XY)_{\mathrm{s}} = (XY + YX)/2$. Clearly, Eq. (6) shows that the matrix $\mathbf{G}$ is the variance-covariance matrix of the multivariate Gaussian distribution function. Moreover, the uncertainty relations can be obtained from Eqs. (6)–(8) as follows:

$$\langle \Delta\mathbf{q}\Delta\mathbf{q}^{\mathrm{T}} \rangle \langle \Delta\mathbf{p}\Delta\mathbf{p}^{\mathrm{T}} \rangle - \langle \mathbf{S} \rangle^2 = \frac{\hbar^2}{4}\mathbf{1}, \tag{9}$$

where we introduce the $3N \times 3N$ real (non-symmetric) matrix $\mathbf{S}$ defined as $S_{j\mu, k\nu} = (\Delta q_{j\mu} \Delta p_{k\nu})_{\mathrm{s}}$, and the $3N \times 3N$ identity matrix $\mathbf{1}$. Now, the trial function in Eq. (2) includes direct correlations between the different degrees of freedom, and preserves the rotational invariance of the WPs without the requirements of the spherical constraints.

The time development of the dynamical variables can be derived from the TDVP.[63–66] The quantum mechanical Lagrangian is now expressed as

$$L \equiv \langle \Psi, t | \left(i\hbar\frac{\partial}{\partial t} - H\right) | \Psi, t \rangle \tag{10}$$

$$= \mathbf{p}_r^{\mathrm{T}}\dot{\mathbf{r}} - \mathrm{Tr}\{\mathbf{G}\dot{\mathbf{K}}\} - H_{\mathrm{ext}}, \tag{11}$$

with the extended Hamiltonian function,

$$H_{\mathrm{ext}} = \frac{1}{2}\mathbf{p}_r^{\mathrm{T}}\mathbf{M}^{-1}\mathbf{p}_r + 2\mathrm{Tr}\{\mathbf{M}^{-1}\mathbf{KGK}\}$$
$$+ \frac{\hbar^2}{8}\mathrm{Tr}\{\mathbf{M}^{-1}\mathbf{G}^{-1}\} + \langle V \rangle, \tag{12}$$

where $\mathbf{M}$ denotes the $3N \times 3N$ diagonal mass matrix of the system; i.e., $M_{j\mu, k\nu} = m_j\delta_{jk}\delta_{\mu\nu}$. Note that H_{ext} in Eq. (12) is equal to the expectation value of the Hamiltonian in Eq. (1). The first term of H_{ext} in Eq. (12) is the kinetic energy associated with the center variables of WPs, and thus it corresponds to the classical kinetic energy. The second term is the homogeneous quadratic form in the generalized momentum (i.e., quadratic in $K_{j\mu, k\nu}$ and linear in $G_{j\mu, k\nu}$), and thus it is regarded as the (generalized) kinetic energy[95] associated with the width variables of WPs. The last two terms in Eq. (12) depend only

on the generalized coordinates and, for the later convenience, will be referred to as the extended potential function V_{ext},

$$V_{\text{ext}} = \frac{\hbar^2}{8} \text{Tr}\{\mathbf{M}^{-1}\mathbf{G}^{-1}\} + \langle V \rangle. \quad (13)$$

The stationary condition of the action integral (i.e., $\delta \int dt L = 0$) leads to the following coupled first-order differential equations:

$$\dot{r}_{j\mu} = \frac{p_{r_{j\mu}}}{m_j}, \quad (14)$$

$$\dot{p}_{r_{j\mu}} = -\frac{\partial \langle V \rangle}{\partial r_{j\mu}}, \quad (15)$$

$$\dot{G}_{j\mu,k\nu} = 2P_{j\mu,k\nu}, \quad (16)$$

$$\dot{K}_{j\mu,k\nu} = -2(\mathbf{K}\mathbf{M}^{-1}\mathbf{K})_{j\mu,k\nu} + F_{j\mu,k\nu}, \quad (17)$$

with the $3N \times 3N$ symmetric matrices $\mathbf{P}$ and $\mathbf{F}$ defined by

$$\mathbf{P} = \mathbf{G}\mathbf{K}\mathbf{M}^{-1} + \mathbf{M}^{-1}\mathbf{K}\mathbf{G}, \quad (18)$$

$$
\begin{aligned}
F_{j\mu,k\nu} &= -\xi_{j\mu,k\nu} \frac{\partial V_{\text{ext}}}{\partial G_{j\mu,k\nu}} \\
&= \frac{\hbar^2}{8}(\mathbf{G}^{-1}\mathbf{M}^{-1}\mathbf{G}^{-1})_{j\mu,k\nu} \\
&\quad - \xi_{j\mu,k\nu} \frac{\partial \langle V \rangle}{\partial G_{j\mu,k\nu}},
\end{aligned} \quad (19)
$$

where $\xi_{j\mu,k\nu} = (1 + \delta_{jk}\delta_{\mu\nu})/2$. With H_{ext} in Eq. (12), these EOMs can be rewritten in the classical Hamiltonian formulation as

$$
\begin{aligned}
\dot{r}_{j\mu} &= \frac{\partial H_{\text{ext}}}{\partial p_{r_{j\mu}}}, \qquad \dot{G}_{j\mu,k\nu} = \xi_{j\mu,k\nu} \frac{\partial H_{\text{ext}}}{\partial K_{j\mu,k\nu}}, \\
\dot{p}_{r_{j\mu}} &= -\frac{\partial H_{\text{ext}}}{\partial r_{j\mu}}, \quad \dot{K}_{j\mu,k\nu} = -\xi_{j\mu,k\nu} \frac{\partial H_{\text{ext}}}{\partial G_{j\mu,k\nu}}.
\end{aligned} \quad (20)
$$

Therefore, the real-time SQ dynamics of the N-particle system in terms of the multi-dimensional thawed GWPs can be expressed by specifying the $9N(N+1)$-dimensional phase space vector consisting of canonical variables,

$$
\begin{aligned}
\mathbf{\Gamma} = (&r_{1x}, r_{1y}, \ldots, r_{Nz}, \\
&G_{1x,1x}, G_{1y,1y}, \ldots, G_{Nz,Nz}, \\
&\sqrt{2}G_{1x,1y}, \sqrt{2}G_{1y,1z}, \ldots, \sqrt{2}G_{Nz,Nx}, \\
&p_{r_{1x}}, p_{r_{1y}}, \ldots, p_{r_{Nz}}, \\
&K_{1x,1x}, K_{1y,1y}, \ldots, K_{Nz,Nz}, \\
&\sqrt{2}K_{1x,1y}, \sqrt{2}K_{1y,1z}, \ldots, \sqrt{2}K_{Nz,Nx}),
\end{aligned} \quad (21)
$$

where the additional factor $\sqrt{2}$ appearing in the off-diagonal elements arises from the symmetric condition of the matrices (e.g., $G_{1x,1y} = G_{1y,1x}$). Note that both the direct correlations between the different degrees of freedom in one particle and the interparticle correlations are entirely included as canonical variables in the phase space vector.

We now introduce the Liouville operator formalism.[33] In the present framework, the time evolution of any arbitrary phase space function $f(\mathbf{\Gamma})$ can be described by the classical Liouville operator,

$$
\begin{aligned}
iL_{\text{ext}} &= -\{H_{\text{ext}}, \ldots\}_{\text{PB}} \\
&= \sum_{j=1}^{N} \sum_{\mu} \left(\frac{\partial H_{\text{ext}}}{\partial p_{r_{j\mu}}} \frac{\partial}{\partial r_{j\mu}} - \frac{\partial H_{\text{ext}}}{\partial r_{j\mu}} \frac{\partial}{\partial p_{r_{j\mu}}} \right) \\
&\quad + \sum_{j=1}^{N} \sum_{\mu} \sum_{k=1}^{N} \sum_{\nu} \xi_{j\mu,k\nu}^2 \\
&\quad \times \left(\frac{\partial H_{\text{ext}}}{\partial K_{j\mu,k\nu}} \frac{\partial}{\partial G_{j\mu,k\nu}} - \frac{\partial H_{\text{ext}}}{\partial G_{j\mu,k\nu}} \frac{\partial}{\partial K_{j\mu,k\nu}} \right),
\end{aligned} \quad (22)
$$

where $\{\ldots, \ldots\}_{\text{PB}}$ is the generalized Poisson bracket in the extended phase space. The time derivative of the function $f(\mathbf{\Gamma})$ is then given by $df/dt = iL_{\text{ext}}f$. For example, the set of Hamilton's EOMs can be simply expressed as $d\mathbf{\Gamma}/dt = iL_{\text{ext}}\mathbf{\Gamma}$. Moreover, it is now straightforward to show that H_{ext} in Eq. (12) is conserved; $dH_{\text{ext}}/dt = iL_{\text{ext}}H_{\text{ext}} = 0$. The time evolution of the function $f(\mathbf{\Gamma}(t)) \equiv f(t)$ from the time t to $t + \Delta t$ is formally described as

$$f(t + \Delta t) = \exp[iL_{\text{ext}}\Delta t]f(t), \quad (23)$$

where $\exp[iL_{\text{ext}}\Delta t]$ is a time propagator.[33] The approximate evaluation of the action of the time propagator will be discussed in Sec. III.

B. Expectation values for potential functions

Next, we discuss the remaining task of evaluating the potential expectation. For some functional forms such as Gaussian functions, it is possible to perform Gaussian integrals analytically and obtain the exact potential expectation $\langle V(\mathbf{q}) \rangle$. Otherwise it is necessary to estimate the potential expectation using appropriate approximation schemes. In the present work, we employ two different approximation schemes to assess the potential expectation: (i) a Gaussian fitting scheme and (ii) Taylor series expansion.[72] Since the former approximation has widely been utilized in various forms, we here focus on describing the latter approximation (see also Appendix A).

We consider the expansion of the general N-body potential $V(\mathbf{q})$ in terms of a Taylor series around $\langle \mathbf{q} \rangle = \mathbf{r}$ as

$$
\begin{aligned}
V(\mathbf{q}) &= V(\mathbf{r} + \Delta\mathbf{q}) \\
&= \exp\left[\Delta\mathbf{q}^{\text{T}} \frac{\partial}{\partial \mathbf{r}'} \right] V(\mathbf{r}') \Big|_{\mathbf{r}'=\mathbf{r}}.
\end{aligned} \quad (24)
$$

Substituting Eq. (24) into $\langle V(\mathbf{q}) \rangle$ and performing the Gaussian integral formally, we can obtain the analytical expression for the potential expectation as

$$\langle V(\mathbf{q}) \rangle = \exp\left[\frac{1}{2} \nabla^{\text{T}} \mathbf{G} \nabla \right] V(\mathbf{r}), \quad (25)$$

where $\nabla \equiv (\partial/\partial \mathbf{r}_1, \ldots, \partial/\partial \mathbf{r}_N)$ denotes the $3N$-dimensional gradient vector with respect to the WP centers. In practice,

the Taylor series of the exponential function of the differential operators in Eq. (25) is truncated at a finite order.[72] Note that the nth-order truncation of the Taylor series of the exponential function in Eq. (25) corresponds to the $2n$th-order expansion of the potential $V(\mathbf{q})$ with respect to $\Delta\mathbf{q}$ in Eq. (24). For example, if we truncate the Taylor series of the exponential function in Eq. (25) at second-order, we can obtain the fourth-order expansion of the potential expectation as

$$\langle V(\mathbf{q})\rangle \simeq \left[1 + \frac{1}{2}\nabla^{\mathrm{T}}\mathbf{G}\nabla + \frac{1}{2!}\left(\frac{1}{2}\nabla^{\mathrm{T}}\mathbf{G}\nabla\right)^2\right]V(\mathbf{r})$$
$$\equiv V^{(0)} + V^{(2)} + V^{(4)}. \qquad (26)$$

Note that the zeroth-order term $V^{(0)}$ in the above expansion depends only on the center coordinates and represents the corresponding classical potential function. In contrast, the higher-order terms $V^{(2)}$ and $V^{(4)}$ depend on both the center and the width coordinates, and give rise to quantum effects; especially, the combination of these higher-order terms and the first term in V_{ext} [Eq. (13)] reproduces the zero-point energy.[72] Note that although the zero-point energy in the present framework is exact only in the case of a harmonic potential, the fourth-order truncation has been found to be accurate enough for the Lippincott-Schroeder potential of anharmonic H-bond.[73]

III. SYMPLECTIC AND TIME-REVERSIBLE INTEGRATOR

From a practical perspective, it is essential to develop stable and efficient numerical algorithms for integrating the EOMs in molecular simulations. Now, it is widely recognized that a symplectic algorithm for the numerical integration of the canonical EOMs has an outstanding advantage that the secular deviation of the total energy is extremely suppressed.[33, 61, 62, 90–93] In this section, we derive the explicit symplectic algorithm with the time reversibility for the numerical integration of the Hamilton's EOMs in Eq. (20).

The presence of a symplectic algorithm is one of the advantages of the Hamiltonian formulation.[61, 62] Computationally, it is desired to find an explicit (non-iterative) symplectic algorithm rather than iterative implicit ones. This is, however, not a trivial task for a non-separable Hamiltonian like H_{ext} in Eq. (12) where the canonically conjugate variables are coupled in the kinetic energy term $2\mathrm{Tr}\{\mathbf{M}^{-1}\mathbf{KGK}\}$. Nonetheless, we can construct the explicit algorithm in the following way. We first decompose the extended Hamiltonian in Eq. (12) into the following two sub-Hamiltonians:

$$H_{\mathrm{ext}} = H_1 + H_2, \qquad (27)$$

$$H_1 = \frac{1}{2}\mathbf{p}_r^{\mathrm{T}}\mathbf{M}^{-1}\mathbf{p}_r + 2\mathrm{Tr}\{\mathbf{M}^{-1}\mathbf{KGK}\}, \qquad (28)$$

$$H_2 = V_{\mathrm{ext}}. \qquad (29)$$

Then, the Liouville operator in Eq. (22) can be divided into the following two operators:

$$iL_{\mathrm{ext}} = iL_1 + iL_2. \qquad (30)$$

Explicit forms of operators iL_1 and iL_2 are expressed as

$$iL_1 = -\{H_1, \ldots\}_{\mathrm{PB}}$$
$$= \sum_{j=1}^{N}\sum_{\mu}\frac{p_{r_{j\mu}}}{m_j}\frac{\partial}{\partial r_{j\mu}}$$
$$+ 2\sum_{j=1}^{N}\sum_{\mu}\sum_{k=1}^{N}\sum_{\nu}\xi_{j\mu,k\nu}$$
$$\times \left[P_{j\mu,k\nu}\frac{\partial}{\partial G_{j\mu,k\nu}}\right.$$
$$\left. - (\mathbf{KM}^{-1}\mathbf{K})_{j\mu,k\nu}\frac{\partial}{\partial K_{j\mu,k\nu}}\right], \qquad (31)$$

$$iL_2 = -\{H_2, \ldots\}_{\mathrm{PB}}$$
$$= \sum_{j=1}^{N}\sum_{\mu}\left(-\frac{\partial\langle V\rangle}{\partial r_{j\mu}}\right)\frac{\partial}{\partial p_{r_{j\mu}}}$$
$$+ \sum_{j=1}^{N}\sum_{\mu}\sum_{k=1}^{N}\sum_{\nu}\xi_{j\mu,k\nu}F_{j\mu,k\nu}\frac{\partial}{\partial K_{j\mu,k\nu}}. \qquad (32)$$

In order to factorize the time propagator $\exp[iL_{\mathrm{ext}}\Delta t]$, we employ the symmetric Trotter theorem for a single time step Δt.[33, 94] The second-order formula with respect to Δt is expressed as

$$e^{iL_{\mathrm{ext}}\Delta t} \simeq e^{iL_2\Delta t/2}e^{iL_1\Delta t}e^{iL_2\Delta t/2}. \qquad (33)$$

This factorization is a short time approximation in which the error is proportional to $(\Delta t)^3$. The higher-order formulas that retain the time reversibility via the symmetric structure of operators can be obtained in a similar manner.[90]

To begin with, consider the action of the operator $\exp[iL_1\Delta t]$ on the vector $\mathbf{r}$ and the matrices $\mathbf{G}$ and $\mathbf{K}$. The action on $\mathbf{r}$ is as simple as that of a shift operator, whereas that on $\mathbf{G}$ and $\mathbf{K}$ is not. However, the latter can be worked out by employing the following two relations. First, in the time evolution by the sub-Hamiltonian H_1, the matrix $\mathbf{KGK}$ is conserved

$$\exp[iL_1\Delta t]\mathbf{KGK} = \mathbf{KGK}. \qquad (34)$$

Second, in the time evolution of the inverse matrix $\mathbf{K}^{-1}$, only terms up to Δt appear as

$$\exp[iL_1\Delta t]\mathbf{K}^{-1} = \mathbf{K}^{-1} + 2\Delta t\mathbf{M}^{-1}. \qquad (35)$$

From Eqs. (34) and (35), we find

$$\exp[iL_1\Delta t]\mathbf{G} = \mathbf{Z}^{\mathrm{T}}(\Delta t)\mathbf{G}\mathbf{Z}(\Delta t), \qquad (36)$$

$$\exp[iL_1\Delta t]\mathbf{K} = \mathbf{Z}^{-1}(\Delta t)\mathbf{K} = \mathbf{K}(\mathbf{Z}^{\mathrm{T}}(\Delta t))^{-1}, \qquad (37)$$

where the $3N \times 3N$ matrix $\mathbf{Z}(\Delta t)$ is defined by

$$\mathbf{Z}(\Delta t) = \mathbf{1} + 2\Delta t\,\mathbf{KM}^{-1}, \qquad (38)$$

with the $3N \times 3N$ identity matrix $\mathbf{1}$. Note that the matrix $\mathbf{Z}(\Delta t)$ depends on the time step Δt explicitly.

Next, consider the action of the operator $\exp[iL_2\Delta t]$ on the vector $\mathbf{p}_r$ and the matrix $\mathbf{K}$. There is no canonically conjugate pair in the sub-Hamiltonian H_2, and therefore the operator $\exp[iL_2\Delta t]$ can be regarded as the shift operator for $\mathbf{p}_r$ and $\mathbf{K}$. Consequently, the time evolution of $\mathbf{p}_r$ and $\mathbf{K}$ by the sub-Hamiltonian H_2 can be obtained straightforwardly.

Finally, the combined action of the three operators in the second-order Trotter factorization in Eq. (33) leads to the following second-order explicit symplectic algorithm with the time reversibility for integrating the Hamilton's EOMs:

1. Update the vector $\mathbf{p}_r$ and the matrix $\mathbf{K}$ according to

$$p_{r_{j\mu}} \leftarrow p_{r_{j\mu}} - \frac{\partial \langle V \rangle}{\partial r_{j\mu}} \frac{\Delta t}{2}, \qquad (39)$$

$$K_{j\mu,k\nu} \leftarrow K_{j\mu,k\nu} - \xi_{j\mu,k\nu} \frac{\partial V_{\text{ext}}}{\partial G_{j\mu,k\nu}} \frac{\Delta t}{2}. \qquad (40)$$

2. Using the new vector $\mathbf{p}_r$ and the new matrix $\mathbf{K}$, evaluate the matrix $\mathbf{Z}(\Delta t)$ and update the vector $\mathbf{r}$ and the matrices $\mathbf{G}$ and $\mathbf{K}$ according to

$$\mathbf{r} \leftarrow \mathbf{r} + \mathbf{M}^{-1}\mathbf{p}_r\Delta t, \qquad (41)$$

$$\mathbf{G} \leftarrow \mathbf{Z}^{\text{T}}(\Delta t)\mathbf{G}\mathbf{Z}(\Delta t), \qquad (42)$$

$$\mathbf{K} \leftarrow \mathbf{Z}^{-1}(\Delta t)\mathbf{K}. \qquad (43)$$

3. Calculate the new generalized forces using the new vector $\mathbf{r}$ and the new matrix $\mathbf{G}$.

4. Update the vector $\mathbf{p}_r$ and the matrix $\mathbf{K}$ according to

$$p_{r_{j\mu}} \leftarrow p_{r_{j\mu}} - \frac{\partial \langle V \rangle}{\partial r_{j\mu}} \frac{\Delta t}{2}, \qquad (44)$$

$$K_{j\mu,k\nu} \leftarrow K_{j\mu,k\nu} - \xi_{j\mu,k\nu} \frac{\partial V_{\text{ext}}}{\partial G_{j\mu,k\nu}} \frac{\Delta t}{2}. \qquad (45)$$

Note that the symbol "$\leftarrow$" indicates that the variables on the left-hand side are overwritten by those on the right-hand side in a computer program.

It should be noted that, as in the usual classical MD simulations, we can utilize a multiple time-scale algorithm in order to reduce the computational costs since the present integration scheme is based upon the Liouville operator formalism.[33,94] For instance, we can achieve it by separating the potential expectation $\langle V \rangle$ into the rapidly varying intramolecular interactions with a small time step $\delta\tau$ and the slowly varying intermolecular interactions with a large time step $\Delta\tau = n\delta\tau$ using the further Trotter factorization of the propagator.[33,94]

IV. COMPUTATIONAL DETAILS

A. Single-particle approximation

Thus far, we have discussed the real-time SQ dynamics of the N-particle system in terms of the multi-dimensional thawed GWPs in which correlations between the different degrees of freedom are fully taken into account by introducing the off-diagonal matrix elements. In this framework, the $3N$-dimensional quantum system is variationally approximated as the $9N(N+1)$-dimensional classical Hamiltonian system. Although the present theory is more accurate than the previous SQGWP theory in this regard, there exist two drawbacks: an expensive computational cost and complexity of analysis. Since the number of degrees of freedom in the matrices $\mathbf{G}$ and $\mathbf{K}$ scales with N^2, and the matrix operations (i.e., the matrix inversion and multiplication) at each time step scale with N^3, the required computational cost soon becomes prohibitive for condensed phase simulations. In addition, it is generally a nontrivial task to extract a small number of essential modes characterizing a target phenomenon from numerous degrees of freedom in such $\sim N^2$-dimensional systems when we analyze nuclear quantum effects from microscopic viewpoints.

In order to avoid the above-mentioned drawbacks in the practical SQ simulations, we employ the single-particle approximation in which the matrices $\mathbf{G}$ and $\mathbf{K}$ are reduced to block-diagonal structures by only considering correlations between the different degrees of freedom in the same particle and neglecting the remaining interparticle correlations. As a result, the reduced matrices consist of N blocks of 3×3 real symmetric matrices along the diagonal, and the number of independent degrees of freedom in each of these matrices becomes $6N$. Note that the analogous approximations have previously been suggested within the framework of the non-Hamiltonian formulation.[52,54,59,60,84]

In the single-particle approximation, we assume that the trial wave function of the system can be factorized into a direct product of correlated 3D Gaussian functions as

$$\Psi(\mathbf{q}, t) = \prod_{j=1}^{N} \Psi_j(\mathbf{q}_j, t), \qquad (46)$$

in which each Ψ_j has the same form as Eq. (2) with $N = 1$, representing the WP of the jth particle. The 3D vectors $\Delta\mathbf{q}_j$, $\mathbf{r}_j$, and $\mathbf{p}_{r_j}$ and the 3×3 matrices $\mathbf{A}_j$, $\mathbf{G}_j$, and $\mathbf{K}_j$ are defined accordingly. The rotational invariance of the WPs is still retained in the single-particle approximation due to the existence of the off-diagonal elements in the matrices. Thus, it is possible to describe the anisotropic fluctuations of the jth WP with the rotational invariance in this approximation.

As was done in Sec. II, the TDVP yields the classical Hamilton's EOMs in the extended phase space. The extended Hamiltonian is now given by

$$H_{\text{ext}} = \sum_{j=1}^{N} \left[\frac{|\mathbf{p}_{r_j}|^2}{2m_j} + \frac{2}{m_j} \text{Tr}\{\mathbf{K}_j\mathbf{G}_j\mathbf{K}_j\} \right] + V_{\text{ext}}, \qquad (47)$$

with the extended potential function,

$$V_{\text{ext}} = \sum_{j=1}^{N} \frac{\hbar^2}{8m_j} \text{Tr}\{\mathbf{G}_j^{-1}\} + \langle V \rangle, \qquad (48)$$

in which the quantum mechanical expectation value $\langle \ldots \rangle$ is defined by the trial function in Eq. (46). Note that the extended Hamiltonian in Eq. (47) is still not separable, and thus the symplectic integrator described in Sec. III is applicable. The resulting set of Hamilton's EOMs is analogous to Eqs. (14)–(17) and Eq. (20) (and thus not presented here).[96]

Consequently, the real-time SQ dynamics of the N-particle system under the single-particle approximation can be expressed by specifying the $18N$-dimensional phase space vector.

In order to clarify the physical meaning of the width coordinates in the single-particle approximation, we consider an eigen-decomposition of the variance-covariance matrix. The jth variance-covariance matrix can be represented in terms of its eigenvalues and eigenvectors

$$\mathbf{G}_j = \mathbf{R}_j^{\mathrm{T}} \widetilde{\mathbf{G}}_j \mathbf{R}_j, \tag{49}$$

where $\widetilde{\mathbf{G}}_j \equiv \mathrm{diag}\,(\lambda_{jx}, \lambda_{jy}, \lambda_{jz})$ is the diagonal matrix whose elements are composed of the eigenvalues, and $\mathbf{R}_j$ is the rotation (or orthogonal) matrix consisting of the eigenvectors, which transforms a 3D Cartesian coordinate vector in the space-fixed axes into that in the principal axes. Then, the rotation matrix $\mathbf{R}_j$ can be expressed in terms of the Euler angles $\{\phi_j, \theta_j, \psi_j\}$ in the usual manner.[33,95] As a result, the width coordinates $\{G_{jxx}, G_{jyy}, G_{jzz}\}$ and $\{\sqrt{2}G_{jxy}, \sqrt{2}G_{jyz}, \sqrt{2}G_{jzx}\}$ are transformed into the generalized coordinates $\{\lambda_{jx}, \lambda_{jy}, \lambda_{jz}\}$ and $\{\phi_j, \theta_j, \psi_j\}$; here, square roots of the eigenvalues correspond to the widths of the ellipsoidal GWPs (EGWPs) in the principal axes, and the Euler angles represent the rotational degrees of freedom of the EGWPs.

In the eigen-decomposition representation, the extended Hamiltonian in Eq. (47) is rewritten as

$$H_{\mathrm{ext}} = \sum_{j=1}^{N} \sum_{\mu} \left[\frac{p_{r_{j\mu}}^2}{2m_j} + \frac{2\lambda_{j\mu}}{m_j} p_{\lambda_{j\mu}}^2 + \frac{l_{j\mu}^2}{2I_{j\mu}} \right] + V_{\mathrm{ext}}, \tag{50}$$

with the extended potential function,

$$V_{\mathrm{ext}} = \sum_{j=1}^{N} \sum_{\mu} \frac{\hbar^2}{8 m_j \lambda_{j\mu}} + \langle V \rangle, \tag{51}$$

where $p_{\lambda_{j\mu}}$ and $l_{j\mu}$ denote the canonically conjugate momentum of the eigenvalue $\lambda_{j\mu}$ and the angular momentum in the principal frame, respectively. Here, the effective moments of inertia $\{I_{jx}, I_{jy}, I_{jz}\}$ in Eq. (50) are defined by[97]

$$
\begin{aligned}
I_{jx} &= m_j \frac{(\lambda_{jy} - \lambda_{jz})^2}{\lambda_{jy} + \lambda_{jz}}, \\
I_{jy} &= m_j \frac{(\lambda_{jz} - \lambda_{jx})^2}{\lambda_{jz} + \lambda_{jx}}, \\
I_{jz} &= m_j \frac{(\lambda_{jx} - \lambda_{jy})^2}{\lambda_{jx} + \lambda_{jy}}.
\end{aligned}
\tag{52}
$$

Note that the angular momenta $\{l_{jx}, l_{jy}, l_{jz}\}$ in Eq. (50) are not canonically conjugate momenta of Euler angles; indeed, the conjugate momenta $\{p_{\phi_j}, p_{\theta_j}, p_{\psi_j}\}$ are related to the angular momenta as

$$
\begin{pmatrix} p_{\phi_j} \\ p_{\theta_j} \\ p_{\psi_j} \end{pmatrix} = \begin{pmatrix} \sin\theta_j \sin\psi_j & \sin\theta_j \cos\psi_j & \cos\theta_j \\ \cos\psi_j & -\sin\psi_j & 0 \\ 0 & 0 & 1 \end{pmatrix} \begin{pmatrix} l_{jx} \\ l_{jy} \\ l_{jz} \end{pmatrix}.
\tag{53}
$$

Now, the physical meaning of the kinetic energy in the extended Hamiltonian in Eq. (50) is obvious; the total kinetic energy is composed of (i) the translational kinetic energy

of the EGWPs corresponding to the classical kinetic energy, (ii) the vibrational kinetic energy representing the spreading motions of the EGWPs, and (iii) the angular kinetic energy describing the rotational motions of the EGWPs.

In molecular liquids, a single-molecule approximation that includes all the intramolecular correlations but disregards the intermolecular correlations would be more appropriate than the single-particle approximation. It would also be reasonable to examine intermediate approximations which include some of intramolecular correlations: for example, a water model that consists of 6×6 and 3×3 blocks by introducing correlations between the hydrogen atoms within the same molecule in addition to the intraparticle correlations and by neglecting the remaining interparticle correlations (i.e., the intramolecular O–H and intermolecular correlations). Nevertheless, we employ only the single-particle approximation in the current work as a first approximation incorporating the anisotropy of the GWPs, and concentrate exclusively on the comparison of it with the corresponding spherical and classical approximations.[98]

B. Flexible SPC water model

The previous applications of the SQGWP theory to liquid water were performed using the SPC/Fd model[74,75] developed by Dang and Pettitt[99] and the q-SPC/Fw model[76] developed by Voth and co-workers.[100] In these flexible and non-polarizable water models, the interaction of the intramolecular O–H stretch is described by a simple harmonic potential.[101] As a result, nuclear quantum effects yield a structural shift toward shorter O–H bond lengths in liquid water.[74,76] However, these results are inconsistent with the recent experimental observation which has indicated that the average O–H bond length in liquid H_2O is larger than the average O—D bond length in liquid D_2O by approximately 3%,[15] and also with several theoretical results.[27,29,43]

Manolopoulos and co-workers have recently found the competition between intra- and intermolecular quantum effects in liquid water using imaginary-time PI and RPMD simulations with the q-TIP4P/F model including an anharmonic intramolecular O–H interaction; that is, intramolecular zero-point fluctuations arising mainly from the anharmonic O–H stretching motion increase the average O–H bond length and the average molecular dipole moment, and then result in stronger intermolecular interactions, whereas intermolecular quantum fluctuations disorder the H-bond network.[43] Note that only the latter quantum effects have long been focused on since most of the previous works are based on a rigid-body model[26] or a flexible model with a harmonic O–H stretching potential.[100] Then, competing nuclear quantum effects in H-bond systems have systematically been investigated using imaginary-time *ab initio* PI simulations.[30] Now, these studies shed light on the importance of the anharmonicity of the O–H stretch in quantum simulations of water.[31,32]

In the present work, we employed the anharmonic flexible SPC (f-SPC) model developed by Toukan and Rahman[102] instead of the SPC/Fd and q-SPC/Fw models in order to take into account the anharmonic O–H interaction and to avoid

technical complexities of quantizing the bending potential function depending explicitly on the H–O–H angle.[103] In this latter respect, the merit of this model for our SQMD scheme lies in the fact that all the potential functions are described in terms of the distances between particles; the intramolecular interactions for the Jth molecule are given by

$$V_{\text{intra}} = V_{\text{stretch}}(r_{\text{OH}_1}) + V_{\text{stretch}}(r_{\text{OH}_2})$$
$$+ V_{\text{bend}}(r_{\text{HH}}) + V_{\text{cross}}(r_{\text{OH}_1}, r_{\text{OH}_2}, r_{\text{HH}}), \quad (54)$$

where r_{OH} and r_{HH} indicate the O–H and H–H distances in the Jth water molecule, respectively. The potential functions V_{stretch}, V_{bend}, and V_{cross} denote the anharmonic quartic potential for the O–H stretching,[104] the simple harmonic potential for the H–O–H bending, and the cross term describing coupling between the internal coordinates in the quadratic form, respectively.[102] Note that the simple harmonic form of V_{stretch} has also been proposed in the original f-SPC model,[102] which will be referred to as the harmonic f-SPC model. This harmonic model has been used in a previous PIMD simulation study,[105] to which we will compare our results in Sec. V A. The intermolecular part of this model, V_{inter}, consists of a 12-6 Lennard-Jones (LJ) potential between oxygen atoms, V_{LJ}, and an electrostatic Coulomb potential between the point charges on atoms, V_{el}.[102]

In order to evaluate the potential expectation in the f-SPC model, we adopted the Gaussian fitting scheme for the anharmonic quartic stretching potential (V_{stretch}), and the fourth-order Taylor expansion [Eq. (26)] for the remaining intramolecular potential functions (V_{bend} and V_{cross}) and the intermolecular potential functions (V_{LJ} and V_{el}).

C. Semiquantal molecular dynamics simulations

We applied the present theory to liquid water under the single-particle approximation, in which both the hydrogen and oxygen atoms were treated as the EGWPs. Despite the fact that the hydrogen atoms play a central role in nuclear quantum effects due to the lightest atomic mass, a recent experimental investigation has shown that quantum effects of the oxygen atoms are also non-negligible in the H-bond structure of water under ambient conditions.[14] This experimental finding has motivated us to quantize all the atoms in water.[76]

The SQMD simulations were performed with the use of the f-SPC model in the microcanonical (NVE) ensemble at a density of 0.997 g cm^{-3} and a target temperature of 298 K with 256 water molecules in a cubic simulation box in which periodic boundary conditions were applied using the minimum image convention. The classical part of the long-range electrostatic interaction, $V_{\text{el}}^{(0)}$, was calculated using the standard Ewald summation, whereas the remaining intermolecular interactions (i.e., $V_{\text{el}}^{(2)}$, $V_{\text{el}}^{(4)}$, and the LJ interactions) were spherically truncated with the use of the smooth function[106] at the cutoff distance of half the box length (i.e., 9.87 Å). The numerical integration of the Hamilton's EOMs was performed using the time-reversible second-order explicit symplectic integrator (SI2) proposed in Sec. III with a time step of $\Delta t = 0.04$ fs. Note that although the time step used here is relatively small due to the fast fluctuations of the WP width

variables of the hydrogen atoms, it is found that even larger time steps (e.g., 0.10 fs) also enable us to obtain stable trajectories as described in Appendix B. The initial conditions of the WP center variables $\{\mathbf{r}_j\}$ and $\{\mathbf{p}_{r_j}\}$ were obtained from the corresponding classical trajectory, and those of the WP width momenta $\{\mathbf{K}_j\}$ were chosen as the zero matrices in order to satisfy the minimal uncertainty at the initial time,[69] whereas those of the WP width coordinates $\{\mathbf{G}_j\}$ were determined by optimizing the extended potential function [Eq. (48)] to introduce the least quantal effects at this time.[69] In the optimization process, the conjugate gradient method was performed using a Cholesky decomposition of $\{\mathbf{G}_j\}$ so that the positive definiteness is automatically assured,[107] instead of implementing constrained optimization. For comparison, we also carried out the additional SQMD simulation using the spherical GWPs (SGWPs) adopted in our previous studies[74–76] and the corresponding classical MD simulation with a time step of $\Delta t = 0.10$ fs under otherwise identical conditions described above.

The methodology for generating statistical mechanical ensembles in the extended phase space has not been completely understood.[80] In the present study, we employed the equilibration method used in the previous simulations,[74–76] in which we adjust the classical degrees of freedom by rescaling only classical velocities and then compute NVE trajectories in the absence of the thermostat. In this equilibration process, other degrees of freedom freely evolve according to the time propagator. After sufficiently long equilibration in this way, the system reaches the thermal equilibrium state due to heat conduction between the different degrees of freedom in the extended phase space. In this simulations, equilibrium NVE trajectories were calculated for 1 ns during which the structural and dynamical properties were computed, after the careful cooling and equilibration runs for more than 200 ps.

V. RESULTS AND DISCUSSION

A. Static equilibrium properties

We first compare the ensemble-averaged static monomer properties in liquid water obtained from SQ and classical simulations listed in Table I: the O–H bond length r_{OH}, the H–O–H bond angle θ_{HOH}, and the molecular dipole moment μ. The monomer properties in the SQMD simulations were calculated from the corresponding expectation values. Clearly, there are significant differences in the average geometries between the SQ and classical models. The O–H bond lengths of the EGWP and SGWP models are greater than that of the classical model by approximately 0.034 and 0.041 Å, respectively. In addition, the H–O–H bond angle of the EGWP model is larger by 1.4°, whereas that of the SGWP model is smaller by 0.5° when compared to its classical counterpart. As a result of these structural changes, the average molecular dipole moments of the EGWP and SGWP models become larger than the classical one by 1.7% and 4.9%, respectively.

In order to evaluate the contribution of intramolecular zero-point fluctuations to the quantum geometric changes of water molecules, we calculated the optimized monomer

TABLE I. Ensemble-averaged static monomer properties in liquid water obtained from the SQ and classical simulations with the f-SPC model. Optimized monomer properties of the isolated water molecule obtained from the SQ simulations are also listed alongside the classical geometric parameters for the f-SPC model. The number in parentheses represents the standard errors in the final digits.

Model	System	r_{OH} (Å)	θ_{HOH} (deg)	μ (D)
EGWP	Liquid	1.0565(1)	106.99(1)	2.4776(1)
SGWP	Liquid	1.0638(1)	105.08(1)	2.5544(1)
Classical	Liquid	1.0225(1)	105.56(1)	2.4353(1)
EGWP	Gas	1.0248	110.46	2.3030
SGWP	Gas	1.0352	109.07	2.3729
Classical[a]	Gas	1.0000	109.47	2.2740

[a]Reference 102.

properties in an isolated water molecule using the SQ models; the results are listed in Table I alongside the geometric parameters for the f-SPC model. It is obvious that, despite the absence of surrounding molecules, the structural differences between the SQ and classical models in gas phase are comparable to those in liquid, indicating that nuclear quantum effects on the average monomer geometry mainly arise from the intramolecular zero-point fluctuations. By comparing the EGWP and SGWP models, we can also find that the anisotropy of WPs slightly reduces the quantum elongation of the O–H distance and gives rise to the opposite structural shift of the H–O–H angle (see Table I). Therefore, the quantum geometry resulting mainly from the intramolecular zero-point energy is sensitive to the anisotropic fluctuations of WPs.

The quantum elongation of the O–H bond length observed in the present study is now consistent with the experimentally observed isotope effect already mentioned in Sec. IV B,[15] and also with some of the previous theoretical results.[27,29,43] In contrast, the high sensitivity of the H–O–H bond angle to the nuclear quantization is inconsistent with the theoretical result which has shown that the average bond angle in the quantum liquid obtained from PI simulations with the q-TIP4P/F model is slightly smaller than in the corresponding classical liquid by only 0.1°.[43] In addition, the analogous result for the water monomer has been reported using PI simulations combined with *ab initio* molecular orbital theory.[28] This discrepancy may stem from the current approximation level of the GWPs, or from the difference in the potential functions. Further investigation will be required to clarify this issue.

In order to quantify nuclear quantum effects on the local H-bond structure in liquid water, we next consider the radial distribution functions (RDFs). Figure 1 shows the O–O, O–H, and H–H RDFs of liquid water calculated from the expectation values using the SQ models (see also Appendix D), along with those obtained from the classical model and those fitted to experimental x-ray[108] and neutron[109] diffraction data in reciprocal space using the reverse Monte Carlo (RMC) method without H-bond constraints.[110] Here, we mainly focus on the O–H RDF (Fig. 1(b)) since its intramolecular and the first intermolecular peaks are directly associated with the covalent bond and H-bond, respectively, which can provide the most fundamental information on the local structures of water. In the intramolecular region of the O–H RDF, both the EGWP
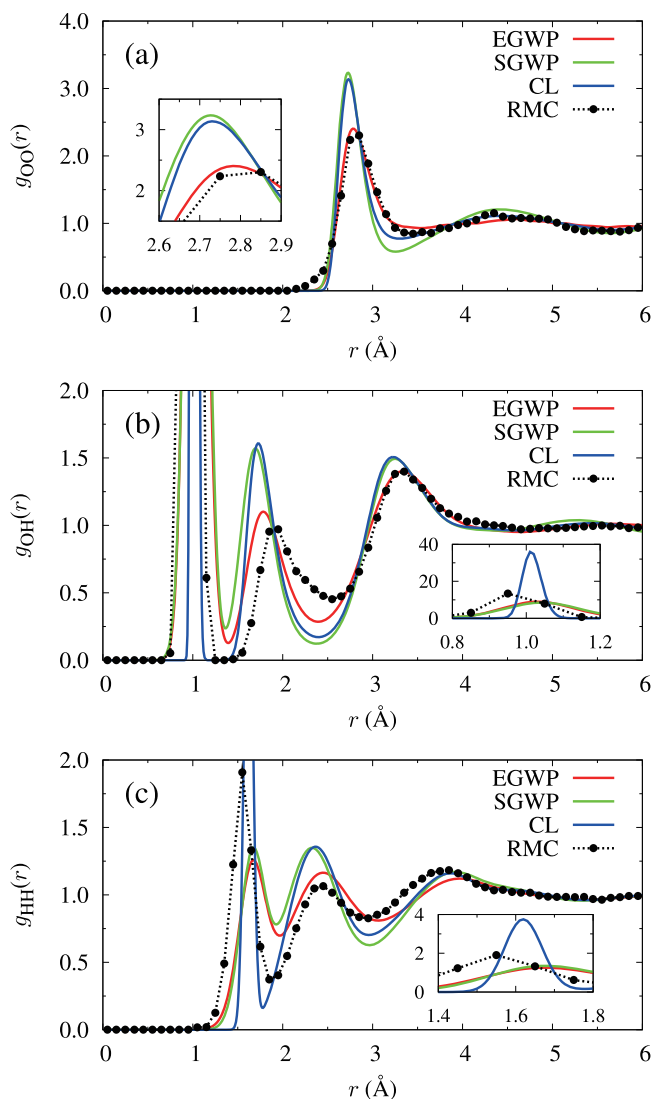

FIG. 1. Radial distribution functions (RDFs) for (a) O–O, (b) O–H, and (c) H–H atom pairs of liquid water calculated from the expectation values using the SQ models. Also shown are the RDFs obtained from the classical (CL) model and those fitted to experimental x-ray (Ref. 108) and neutron (Ref. 109) diffraction data in reciprocal space using the reverse Monte Carlo (RMC) method without H-bond constraints (Ref. 110). The insets show the magnifications of the corresponding first peaks.

and SGWP models yield the significantly broader distributions than the classical one, and the difference between the SQ models is rather minor. In the intermolecular region of the O–H RDF, the first peak of the EGWP model, which directly represents the local H-bond, exhibits a considerable reduction of the height and a slight shift of the position toward the larger distance compared to the classical peak: 1.10 located at 1.78 Å and 1.61 at 1.73 Å for the EGWP and classical models, respectively. In contrast, the first peak of the SGWP model has the almost identical intensity (1.57) and the position shifted toward the slightly shorter distance (1.70 Å) compared to the corresponding classical peak. The similar behavior is also observed in the O–O and H–H RDFs; for example, the first peak heights of the O–O RDFs for the EGWP, SGWP, and classical models give values of 2.40, 3.23, and 3.14, which are located at 2.78, 2.73, and 2.73 Å, respectively (Fig. 1(a)).
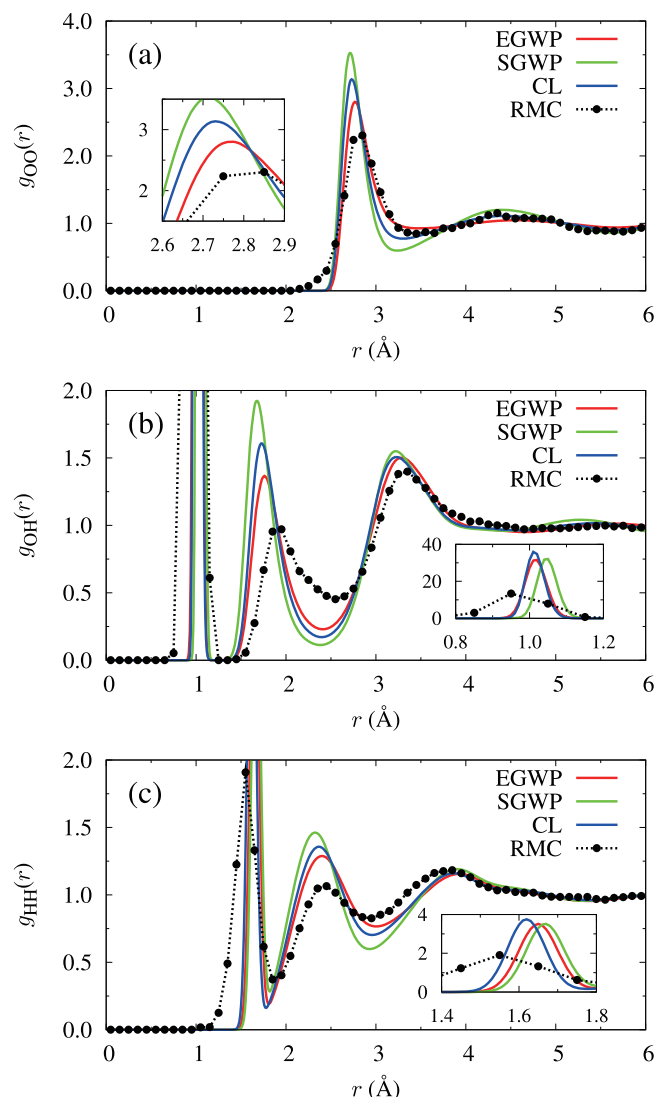
FIG. 2.   Same as Fig. 1 except that the RDFs for the SQ models are calculated with respect to the WP centers.

These results indicate that the anisotropy of WPs has a strong impact upon the local H-bond structure.

The differences in the RDFs between the SQ and classical models stem from both the broadening of distributions due to the WP delocalization and the structural changes of the WP centers.[76] In order to assess the latter contribution, we also calculated the O–O, O–H, and H–H RDFs with respect to the WP centers using the SQ models (i.e., the zeroth-order truncation of the Taylor series around the WP centers in Eq. (D1)); the results are displayed in Fig. 2. In the intramolecular region of the O–H RDF, both the EGWP and SGWP models have the sharp distributions comparable to the classical one due to the lack of the WP spreading effects (Fig. 2(b)). Interestingly, the deviation between the SQ models is now clearer, indicating that the combination of the difference in the WP centers and that in the WP widths results in the almost identical full-order distributions between the SQ models in this radial region (see the insets of Figs. 1(b) and 2(b)). In the intermolecular region of the O–H RDF, the opposite quantum behavior can be seen between the

SQ models in comparison with the classical one; that is, the first intermolecular peak of the EGWP model has the smaller height (1.37) and the position shifted toward the larger distance (1.76 Å), whereas that of the SGWP model has the larger height (1.96) and the position shifted toward the shorter distance (1.68 Å) when compared to the classical peak (1.61 located at 1.73 Å). The analogous behavior can also be observed in the intermolecular peaks of the O–O and H–H RDFs. These results mean that the anisotropic fluctuations of the WPs play a critical role in the quantum disruption of the H-bond network formed by the WP centers, which competes with the stronger intermolecular interactions coming from the larger molecular dipole moments (Table I).

In the case of the EGWP model, the contribution of the WP delocalization and the disorder in the WP centers gives rise to the significantly less structured RDFs (Fig. 1) which are in reasonable agreement with the reference results obtained from the RMC method[110] which can optimally reproduce the experimental x-ray[108] and neutron[109] data in reciprocal space,[111] except that the intramolecular peaks for the EGWP model are lower and the positions of these peaks are at longer distances than those from the RMC method probably due to the lack of the intramolecular quantum correlations particularly between the hydrogen atoms. In contrast, the cancellation between the broadening of the distribution and the overstructuring of the WP centers leads to the classical-like intermolecular peaks for the SGWP model (Fig. 1), which are apparently incompatible with the experimental data. Therefore, these findings highlight the importance of incorporating the anisotropy into the WPs in liquid water described by potential models accounting for the O–H anharmonicity. In order to further improve the agreement with the experiments, the current EGWP model (i.e., the single-particle approximation) could be remedied by adopting more general GWPs such as the single-molecule approximation described in Sec. IV A.

The direct comparison between the real-time SQMD and imaginary-time PIMD simulations for the same potential model is essential to obtain a more quantitative assessment of the accuracy of the static properties in the present approximation. The numerically exact RDFs obtained from the imaginary-time PIMD simulation with the harmonic f-SPC model have been reported in Ref. 105, which will provide the benchmark reference with a notion on the difference between the harmonic and anharmonic f-SPC models. It can be seen from Figs. 1–3 of Ref. 105 that the heights of the first intermolecular peaks of the O–O, O–H, and H–H PIMD RDFs give values of approximately 2.72, 1.23, and 1.21, which are located at approximately 2.79, 1.79, and 2.43 Å, respectively, whereas the corresponding peak heights for the EGWP model are 2.40, 1.10, and 1.16, which are located at 2.78, 1.78, and 2.45 Å, respectively (Fig. 1). These underestimates of the peak heights seem to imply that nuclear quantum effects on the local H-bond structures are overestimated in the single-particle approximation. Again, constructing more precise GWPs as well as more appropriate potential model should be done in future in an effort to obtain more rigorous quantum descriptions within the present theoretical framework (see also Sec. VI).
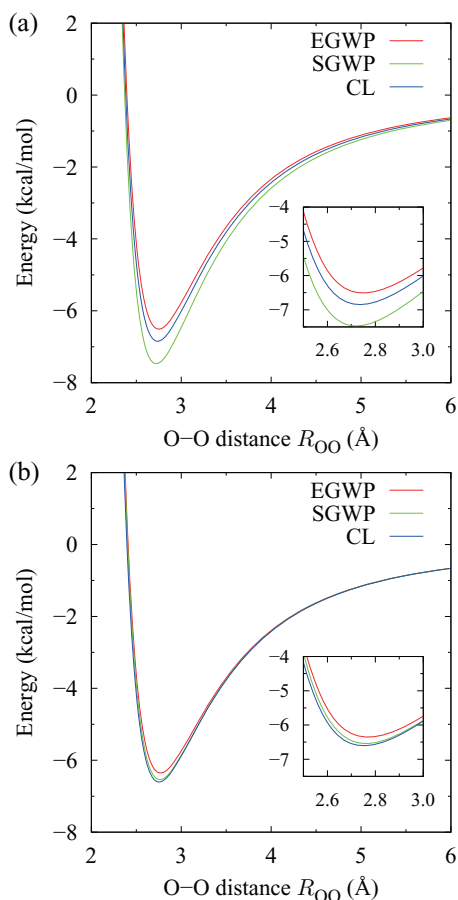
FIG. 3. (a) Optimized energies of the water dimer as a function of the O–O distance obtained from the SQ and classical (CL) simulations without intramolecular constraints and (b) those with the fixed intramolecular geometry (see text), where the energy is defined as the deviation from the energy of two isolated water molecules and the O–O distance is calculated with respect to the WP centers. The insets show the magnifications of the corresponding minimum regions.

To gain further insights into the structural aspects of nuclear quantum effects, we carry out an energetic analysis of an isolated water dimer. Figure 3(a) compares the optimized energies of the water dimer as a function of the O–O distance between the SQ and classical models. Note that this energy is defined as the deviation from the energy of two isolated water molecules,[112] and the O–O distance is calculated with respect to the WP centers. The C_s symmetry configurations of the water dimer[112] are found to be the most stable for all the models over the whole range of O–O distances considered in the current study. It is found that the global minimum which corresponds to the dimer binding energy varies from −6.85 to −6.51 kcal/mol and the location shifts from 2.74 to 2.75 Å when the classical nuclei are quantized by the EGWP model, which is contrary to the behavior of the SGWP model (−7.47 kcal/mol located at 2.72 Å). Surprisingly, the minimum energy path for the SGWP model lies below that for the classical model despite the presence of the intermolecular zero-point energy, for the reasons described next. These energetic profiles are consistent with the first intermolecular peaks of the O–H RDFs for the WP centers plotted in Fig. 2(b); in-

deed, the optimized donor-acceptor separations of the water dimer with respect to the WP centers for the EGWP, SGWP, and classical models are 1.73, 1.67, and 1.72 Å, respectively, which are compatible with the corresponding peak position of the O–H RDFs (Fig. 2(b)).

The energetic differences between the SQ and classical models described above originate from several quantum factors; in particular, one important origin is the intramolecular geometric changes induced by the intramolecular zero-point energy. In order to clarify its role in the intermolecular interactions, we calculated the optimized energies of the water dimer with the constraint in which the intramolecular geometries with respect to the WP centers are fixed at the classical monomer geometry (Table I) so that the molecular dipole moments with respect to the WP centers become equivalent among all the models; the results are depicted in Fig. 3(b) as a function of the O–O distance. We can see that the global minima are −6.35, −6.54, and −6.61 kcal/mol and the minimum positions are 2.77, 2.76, and 2.75 Å for the EGWP, SGWP, and classical models, respectively. The systematic differences (i.e., the destabilization of the H-bond and the elongation of the O–O distance), which are pronounced mostly in the EGWP model, are mainly attributed to the quantization of the intermolecular potential function (i.e., $V_{inter}^{(2)}$ and $V_{inter}^{(4)}$). By comparing Figs. 3(a) and 3(b), it is now evident that the intermolecular zero-point energy make a large contribution toward the destructuring of the H-bond in the EGWP model, while the intramolecular geometric changes with respect to the WP centers are dominant in the SGWP model and thus result in the stabilization of the H-bond.

As has been reported in the previous work, when the Coulomb potential function is quantized by the SGWP model, all the higher-order terms in the Taylor series (i.e., $V_{el}^{(2)}$, $V_{el}^{(4)}$, and so on) are equal to zero due to the spherical symmetry (see the Appendix of Ref. 76); instead, the direct quantization can be performed using the Gaussian integral.[74] In this case, its quantum contribution is characterized by the error function (erf) whose argument consists of the interparticle distance divided by the WP widths. In the present SQMD simulation of liquid water calculated from the SGWP model, it is found that the erf term gives the saturated value of unity (i.e., classical limit) since the WP widths are smaller than the intermolecular separations by more than an order of magnitude; indeed, the deviation (1 − erf) is smaller than 10^{-15} during the 1 ns trajectory, and thus nuclear quantum effects arising directly from the intermolecular Coulomb potential are essentially negligible. In fact, the small quantum differences between the SGWP and classical models shown in Fig. 3(b) stem from the quantization of the intermolecular LJ potential (i.e., $V_{LJ}^{(2)}$ and $V_{LJ}^{(4)}$), and are counterchanged by the stronger intermolecular potential, $V_{inter}^{(0)}$, coming from the intramolecular geometric changes in the SGWP model (Fig. 3(a)). In contrast, the quantization of the intermolecular Coulomb potential has a significant influence on the disordering of the H-bond in the EGWP model as shown in Figs. 3(a) and 3(b). Therefore, the anisotropy of the WPs is indispensable for quantizing the intermolecular Coulomb potential when the WP widths are localized compared to the intermolecular distances by approximately one order of magnitude.

B. H-bond exchange dynamics

Next, we investigate the molecular jump mechanism in the H-bond exchange process which is originally proposed by Laage and Hynes as an elementary mechanism of the collective H-bond network rearrangement in liquid water using classical MD simulations; they suggested that the H-bond donor (O*H*) suddenly performs a large-amplitude angular jump from the initial oxygen acceptor (O^a) toward the final one (O^b) at the intermediate state where the rotating donor forms a symmetric bifurcated H-bond with its initial and final acceptors, and in this way the breaking and forming of H-bonds occur concertedly.[9] Note that the analysis is based on averaged H-bond exchange trajectories in which a large number of H-bond switching events are sampled.[9] Recently, the experimental development of two-dimensional infrared spectroscopy has also provided further insights into the H-bond exchange dynamics of water in solution.[13]

We here focus on nuclear quantum effects on the time development of several structural parameters along the H-bond exchange trajectories: the jump angle θ, the O^{a}O*O^b angle ψ, and the O–O distances for the O*O^a, O*O^b, and O^{a}O^b pairs, where θ is defined as the angle between the projection of the O*H* vector on the O^{a}O*O^b plane and the bisector of ψ. Note that all the structural parameters were calculated with respect to the WP centers in the SQMD simulations. In addition, the time evolution of the WP widths of the H* atom for the EGWP model is also calculated, which is one of the most primary results of the present work. The points at which $\theta = 0$ are taken to be the time origin of the H-bond exchange trajectories (i.e., $t = 0$), and ca. 84 500, 45 100, and 67 000 H-bond exchange events were averaged from the microcanonical simulations of 1 ns for the EGWP, SGWP, and classical models, respectively. The formation of the H-bond was evaluated on the basis of the geometric criteria with respect to the WP centers: the O–O distance smaller than 3.50 Å, the intermolecular O–H distance smaller than 2.45 Å, and the H–O–O angle smaller than 30°.[10]

Figure 4 shows the averaged H-bond exchange trajectories of the jump angle θ and the O^{a}O*O^b angle ψ. It is clear from Fig. 4(a) that nuclear quantum effects on the jump angle θ are relatively minor; in the initial and final H-bond states, both the magnitude of the average value and the standard deviation (SD) for the EGWP model are slightly greater than the classical counterparts by approximately 1°, which is opposite to the behavior for the SGWP model. Each of the results can be reasonably expressed as a sum of two error functions,[13] and is found to be composed of two kinds of angular motions; the faster components which correspond to the angular jumps at the intermediate state have the amplitudes of 50°, 46°, and 48° with a time scale of approximately 120 fs, and the slower reorientational components have the amplitudes of 19°, 17°, and 18° with a time scale of approximately 2 ps for the EGWP, SGWP, and classical models, respectively. The analogous differences in the time development of ψ among the SQ and classical models are found over the whole range of time plotted in Fig. 4(b).

The behavior of ψ in Fig. 4(b) is related to that of the O–O distances displayed in Fig. 5. The averaged H-bond ex-
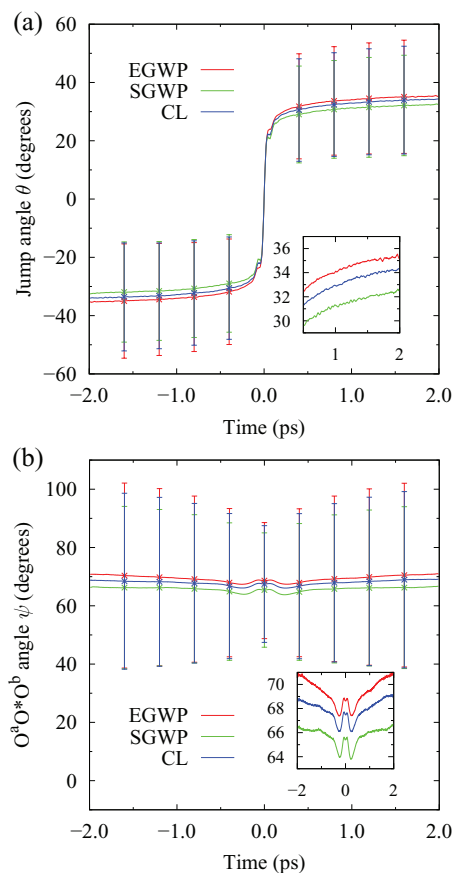

FIG. 4. Averaged H-bond exchange trajectories of (a) the jump angle θ and (b) the O^{a}O*O^b angle ψ. The standard deviations are also plotted as error bars. The insets show the corresponding magnifications.

change trajectories for O*O^a and O*O^b are symmetric with regard to the midpoint $t = 0$ (Fig. 5(a)). In the initial H-bond state ($t < 0$), nuclear quantum effects on the H-bonded O*O^a distance are comparatively small; the time-averaged values from $t = -2.0$ to -0.4 ps are 2.87, 2.83, and 2.84 Å for the EGWP, SGWP, and classical models, respectively. In contrast, the quantum effects are notable for the O*O^b distance in this time region; the slopes of the O*O^b distances within the time range from -2.0 to -0.4 ps, which correspond to the averaged relative velocities of the O^b atoms coming from the second coordination shell, are -0.35, -0.16, and -0.25 Å/ps for the EGWP, SGWP, and classical models, respectively. The analogous quantum effects on the O^{a}O^b distances are also found in Fig. 5(b). In the intermediate H-bond state ($t \simeq 0$), the quantum differences in the O–O distances between the SQ and classical models are relatively small.

Since the present SQMD simulations are based upon the real-time and real-space SQ theory, the dynamical broadenings of the WP widths can be directly monitored. Figure 6 exhibits each component of the WP width fluctuations of the jumping hydrogen atom H* in the body-fixed axes obtained from the averaged H-bond exchange trajectories for the EGWP model; here, the WP width fluctuation $\delta\rho$ is defined as the deviation from the corresponding statistical average,[113] and the body-fixed axes are introduced so that the water molecule lies in the xy plane, with the x-axis along the O*H*
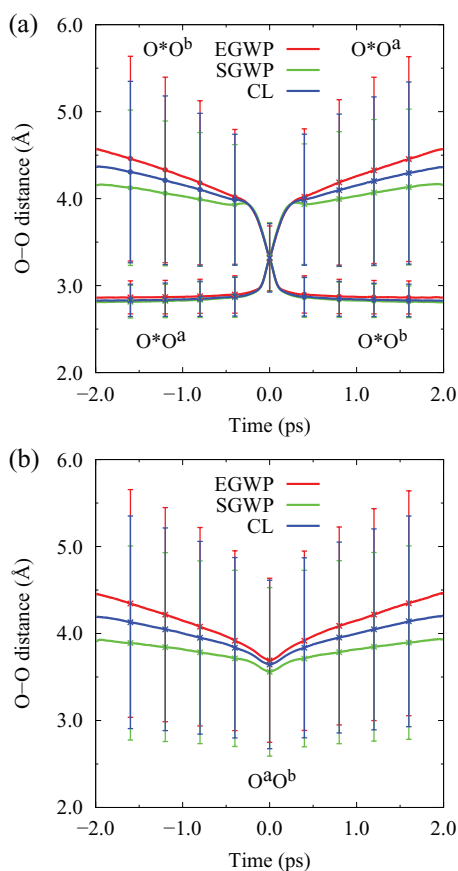
FIG. 5. Averaged H-bond exchange trajectories of (a) the O^*O^a and O^*O^b, and (b) the O^aO^b distances. The standard deviations are also plotted as error bars.

direction and the z-axis pointing to the out-of-plane of the molecule (see Fig. 6). Note that the principal axes of the EGWP of the H^* atom are equivalent to the body-fixed axes on average. It is found that the behavior of the WP width fluctuations is symmetric with respect to $t = 0$; the WP widths along the y- and z-axes shrink compared to the average values in the initial H-bond region and then sharply broaden toward the intermediate state, while that along the x-axis is close to
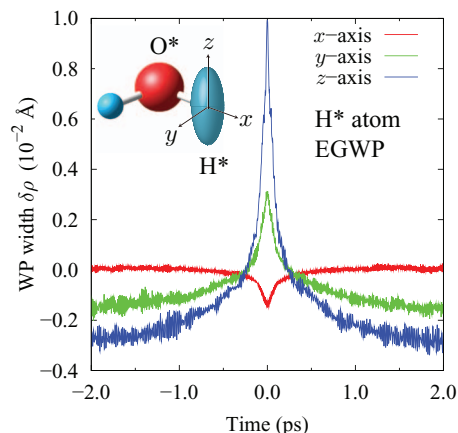

FIG. 6. Averaged H-bond exchange trajectories of the WP width fluctuations of the jumping hydrogen atom H^* in the body-fixed axes obtained from the SQ simulation with the EGWP model. Also shown is the graphical definition of the body-fixed axes for the H^* atom.

the average value in the initial H-bond region and then suddenly shrinks toward the intermediate state. In particular, the WP delocalization along the z-axis is significant; the variation of the WP width along the z-axis for the EGWP model is much larger than that of the isotropic WP width for the SGWP model by approximately two orders of magnitude (see Fig. 8 of Ref. 76). Furthermore, it is obvious from Fig. 6 that the WP of the H^* atom becomes the most anisotropic at the intermediate state. The anisotropic WP width fluctuations at the intermediate state are due to the weaker intermolecular interactions among the bifurcated H-bonds compared to the stable H-bond interactions at the initial and final states; that is, in the absence of the strong local intermolecular interactions, the WP widths along the x- and y-axes at the intermediate state are predominantly affected by the intramolecular stretching and bending interactions, respectively,[114] whereas that along the z-axis is almost immune to the intramolecular interactions owing to the steric effect for this axis and thus significantly broadens just as in the free particle.

C. H-bond number fluctuation

Finally, we analyze nuclear quantum effects on the local H-bond coordination number N_{HB}. The statistical average values of N_{HB} are 3.38, 3.71, and 3.55 for the EGWP, SGWP, and classical models, respectively. These results are consistent with the quantum effects on the structural properties described in Sec. V A (i.e., the destructuring and overstructuring for the EGWP and SGWP models, respectively).

The dynamical aspect of N_{HB} can be obtained from the normalized classical time-correlation functions (TCFs),[115]

$$C_{HB}(t) = \langle \delta N_{HB}(t) \delta N_{HB}(0) \rangle_0 / \langle \delta N_{HB}^2 \rangle_0, \qquad (55)$$

where $\delta N_{HB}(t) = N_{HB}(t) - \langle N_{HB} \rangle_0$, and $\langle \ldots \rangle_0$ denotes the statistical average. Here, although the TCFs computed with respect to the WP centers corresponds to the zeroth-order approximation of the quantum mechanical TCFs (i.e., the classical TCFs), the zero-point energy is primarily introduced in the TCFs since the time development of the WP centers is explicitly affected by the WP width variables. As shown in Fig. 7(a), the TCFs for the EGWP, SGWP, and classical models show the initial fast decay with time scales of approximately 50, 100, and 80 fs, respectively, followed by the slower decay with time constants of approximately 0.5, 1.0, and 0.7 ps, respectively. These results indicate that the anisotropy of the WPs accelerates the decay, whereas the spherical symmetry of the WPs decelerates. The quantum differences in the longer time region are closely related with the deviations of the power spectra in the lower frequency range (see the inset of Fig. 7(a)).

In order to estimate the dynamical WP spreading effects on dynamics of the H-bond number fluctuations, we further calculated $C_{HB}(t)$ with the frozen GWPs (FGWPs) in which only the rotational and translational degrees of freedom of the WPs are allowed to fluctuate and the breathing motions of the WPs along the principal axes are prohibited; that is, the eigenvalues $\{\lambda_{j\mu}\}$ in Eq. (50) are always fixed at the corresponding statistical average values. In this approximation, the rotational and translational EOMs for the FGWPs can be straightfor-
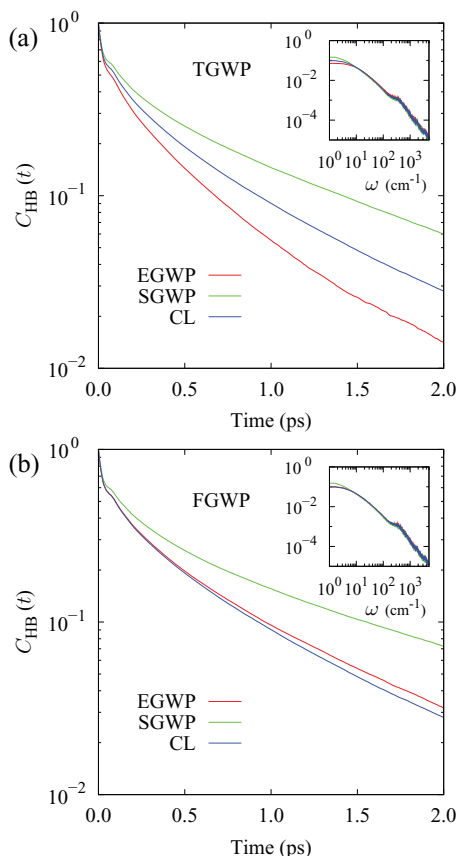
FIG. 7. (a) Normalized time correlation functions of the H-bond number fluctuation obtained from the SQ simulations with the thawed GWPs (TGWPs) and (b) those with the frozen GWPs (FGWPs) in which only the rotational and translational degrees of freedom of the WPs are allowed to fluctuate. Also shown is the classical (CL) result. The insets show the corresponding power spectra in arbitrary units. Notice the logarithmic scales of the axes.

wardly derived from H_{ext} in Eq. (50) in a manner analogous to the derivation of the classical EOMs for a rigid body.[95] Note that we numerically solved the rotational EOMs for the quaternion instead of the Euler angles in the usual manner.[92] As shown in Fig. 7(b), the difference in the decay between the frozen EGWP and classical models is significantly small, while that between the frozen SGWP and classical models is still pronounced and slightly enhanced. Therefore, the dynamical breathing motions of the EGWPs, which include the anisotropic WP delocalization in the H-bond exchange process shown in Fig. 6, give rise to the acceleration of the decay, whereas the spherically symmetric broadenings of the SGWPs play a minor role in the deceleration of the decay.

VI. CONCLUSIONS

In the present paper, we have proposed the novel real-time and real-space SQ theory within the framework of the Hamiltonian formulation using the correlated multi-dimensional thawed GWPs including direct correlations between the different degrees of freedom which are neglected in the previous SQGWP theory. In addition to the classical degrees of freedom (i.e., the WP centers), the variance-covariance matrix elements and the corresponding conjugate

matrix elements are introduced as auxiliary canonical variables. The classical Hamilton's EOMs in the extended phase space have been derived from the TDVP, which has made it possible to perform the real-time and real-space SQMD simulations and to analyze nuclear quantum effects on dynamics in many-body molecular systems in terms of the anisotropic fluctuations of nuclear WPs with preserving the rotational invariance. The form of the trial GWP function is different from the well-known Heller's one but was originally suggested in the field of nuclear physics,[89] whose application to realistic molecular systems with the explicit derivation of the canonical EOMs and the symplectic integrator algorithm (see next) has been first reported to our knowledge.

Based on the Liouville operator formalism in the extended phase space, we have also developed the explicit symplectic algorithm with the time reversibility for integrating the Hamilton's EOMs. The time-reversible symplectic algorithm guarantees the preservation of the phase space volume, the conservation of the approximate Hamiltonian, and the time reversibility, during the time evolution of the phase space vector. As a result, it can provide the long-time stability of trajectories in the SQMD simulations with even larger time steps (see also Appendix B).

In order to reduce the number of total degrees of freedom in the extended phase space which is proportional to N^2, we have adopted the single-particle approximation in which the variance-covariance matrix and the corresponding conjugate matrix are reduced to block-diagonal forms by only taking into account correlations between the different degrees of freedom in one particle and disregarding the remaining inter-particle correlations. In this approximation, we explored the physical meaning of the generalized coordinates in the extended phase space by means of the eigen-decomposition of the variance-covariance matrix; thus, the SQ particles can be regarded as the EGWPs which have the translational, the vibrational, and the rotational degrees of freedom.

Employing the single-particle approximation, we have carried out the SQMD simulations of liquid water with the potential model including the O–H anharmonicity. The advantage of describing real-time and real-space dynamics allows us to directly quantize the H-bond exchange trajectories in the present SQMD simulations. As a result, the significant WP delocalization, particularly along the out-of-plane direction, of the jumping hydrogen atom has been found at the intermediate state in the H-bond exchange process, indicating the anisotropic nature of nuclear WPs in the H-bond network reorganization of liquid water.

In the current methodology, difficulty in quantizing general potential functions restricts ourselves to selecting the specific potential models compatible with the Gaussian integrals in Cartesian coordinates, and thus developments of precise and compact representation of the potential in a suitable form for this methodology should be accomplished. From this standpoint, a simple WP modeling of electrons in chemical bonding has recently been exploited using floating and breathing SGWPs, and reasonably accurate molecular potential energy surfaces have been obtained.[85,86] The unification of this electron WP modeling and the current SQGWP theory enables us to perform *ab initio* SQMD simulations

of molecular systems and processes including chemical reactions, and further work along these lines is certainly to be desired. Moreover, developing the analogous theoretical framework for an approximate assessment of quantum mechanical TCFs (e.g., the standard and Kubo-transformed TCFs) would provide more quantitative information on quantum dynamical properties, for instance, the self-diffusion coefficient of the benchmark systems such as liquid *para*-hydrogen[116–120] and the infrared linear absorption spectrum of liquid water.[38,39,43,44,46,47] The application of it to computing the multi-time correlation function[21–24,121–123] would also be of interest.

ACKNOWLEDGMENTS

APPENDIX A: GAUSSIAN FITTING SCHEME

We here present an efficient numerical scheme to evaluate Gaussian integrals in the potential expectation in Eq. (13), assuming the total potential function of the system to be a sum of pair potential functions as

$$V(\mathbf{q}) = \sum_{j>k}^{N} V_{jk}(q_{jk}), \tag{A1}$$

where $V_{jk}(q_{jk}) \equiv V_{jk}(|\mathbf{q}_j - \mathbf{q}_k|)$ denotes the pair potential function depending only on the distance between the jth and kth atoms. Based on the facts that any central potential can be fitted by a sum of Gaussian functions centered at the origin and that a Gaussian in the distance q_{jk} centered at the origin remains to be a Gaussian after transformation into the Cartesian coordinates, the pair potential can be approximated in terms of a sum of Gaussians as[52,54,59,60,84]

$$V_{jk}(q_{jk}) = \sum_{p} c_{jk}^{(p)} \exp\left(-\alpha_{jk}^{(p)} q_{jk}^2\right), \tag{A2}$$

with fitting parameters $\{c_{jk}^{(p)}\}$ and $\{\alpha_{jk}^{(p)}\}$. The evaluation of the potential expectation is now reduced to that of the following Gaussian integral:[59,84]

$$\left\langle \exp\left(-\alpha_{jk}^{(p)} q_{jk}^2\right)\right\rangle = \left\{\det\left(2\alpha_{jk}^{(p)}\mathbf{B}_{jk} + \mathbf{I}\right)\right\}^{-1/2}$$
$$\times \exp\left[-\mathbf{r}_{jk}^{\mathrm{T}}\mathbf{C}_{jk}\mathbf{r}_{jk}\right], \tag{A3}$$

with the 3D vector $\mathbf{r}_{jk} = (\mathbf{r}_j - \mathbf{r}_k)$, the 3×3 identity matrix $\mathbf{I}$, and the 3×3 matrices $\mathbf{B}_{jk}$ and $\mathbf{C}_{jk}$ defined by

$$\mathbf{B}_{jk} = \mathbf{G}_{jj} + \mathbf{G}_{kk} - \mathbf{G}_{jk} - \mathbf{G}_{kj}, \tag{A4}$$

$$\mathbf{C}_{jk} = \alpha_{jk}^{(p)}\mathbf{I} - 2\left(\alpha_{jk}^{(p)}\right)^2\left(2\alpha_{jk}^{(p)}\mathbf{I} + \mathbf{B}_{jk}^{-1}\right)^{-1}, \tag{A5}$$

where $\mathbf{G}_{jk}$ is the corresponding 3×3 block of the matrix $\mathbf{G}$.[59,84] It is possible to straightforwardly obtain analytical expressions for the generalized forces (first-order derivatives with respect to the generalized coordinates).[96]

APPENDIX B: CONSERVED HAMILTONIAN

In the time evolution described by the symplectic algorithm based upon factorized propagators with a finite time step, there exists a formally exact conserved quantity called a shadow Hamiltonian in a form slightly modified from the original Hamiltonian. This in general guarantees nondivergent stability in large-scale and long-time MD simulations.

In the second-order symplectic algorithm proposed in Sec. III, the shadow Hamiltonian up to order $(\Delta t)^2$ is given by[33]

$$\tilde{H}(\boldsymbol{\Gamma}; \Delta t) = H_{\mathrm{ext}}(\boldsymbol{\Gamma}) + \tilde{H}^{(1)}(\boldsymbol{\Gamma})(\Delta t)^2 + O((\Delta t)^4), \tag{B1}$$

where the quantity $\tilde{H}^{(1)}$ is expressed as[96]

$$\tilde{H}^{(1)} = -\frac{1}{24}\{H_2 + 2H_1, \{H_2, H_1\}_{\mathrm{PB}}\}_{\mathrm{PB}}, \tag{B2}$$

with the generalized Poisson bracket [Eq. (22)] and the two sub-Hamiltonians [Eqs. (28) and (29)].

In order to assess the accuracy and the long-time stability of trajectories, we performed the additional SQMD simulations using SI2 and the fourth-order Runge-Kutta method (RK4) with several time steps under otherwise identical conditions described in Sec. IV C. Note that RK4 is neither time-reversible nor symplectic algorithm. It should also be noted that RK4 requires four updates of the generalized forces at each time step, while SI2 requires just one update.

Figure 8 illustrates the time series of the deviation of the extended Hamiltonian in Eq. (47) from its initial value, defined by $\delta H(t) = H_{\mathrm{ext}}(t) - H_{\mathrm{ext}}(0)$, using SI2 and RK4 with a time step of 0.02 fs. It is clear that, in contrast with RK4 that exhibits monotonic energy drift typical of the non-symplectic algorithms, SI2 demonstrates good conservation of H_{ext} for as long as 1 ns. Small fluctuations around the initial value without systematic drift are observed owing to the existence of the shadow Hamiltonian in Eq. (B1). In this case, the SD of the total Hamiltonian is approximately 0.001 kcal/mol, whose
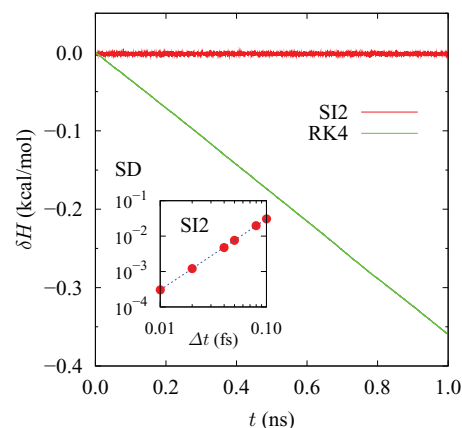
FIG. 8. Time series of the deviation of the total Hamiltonian from its initial value in liquid water calculated from the EGWP model using the time-reversible second-order explicit symplectic integrator (SI2) and the fourth-order Runge-Kutta method (RK4) with a time step of $\Delta t = 0.02$ fs. The inset shows the time step versus the standard deviation (SD) of the total Hamiltonian in kcal/mol using SI2; here, notice the logarithmic scales of the axes. Also shown in the inset is the linear fitting with a slope of 2.00 (dotted line).

ratio to the SD of the classical kinetic energy is approximately 0.0001. Furthermore, the SD of the total Hamiltonian is found to be proportional to $(\Delta t)^2$ as expected (see the inset of Fig. 8). Therefore, the SI2 developed in Sec. III is confirmed to be a robust and efficient integration scheme for long-time SQMD simulations, yielding the time evolution confined on the constant energy hypersurface described by the shadow Hamiltonian in Eq. (B1) and preserving the phase space volume.

APPENDIX C: PRESERVATION OF ZERO-POINT ENERGY

It has been found that the diffusion coefficient of liquid water obtained from the RPMD simulation with the q-TIP4P/F model under ambient conditions is only slightly larger than the classical counterpart due to the competition between intra- and intermolecular quantum effects as described in Sec. IV B,[43] whereas that obtained from the LSC-IVR simulation under identical conditions is three times larger than the classical one.[44] This discrepancy has been ascribed to the unphysical leakage of initially quantized zero-point energy from the intramolecular to the intermolecular modes in the LSC-IVR simulation where completely classical trajectories are developed from an initially quantized phase space distribution.[44] Here, we confirm that the current methodology can avoid the leakage of the zero-point energy.

Figure 9 shows the time development of the intra- and intermolecular potential energies obtained from the SQMD simulation with the EGWP model; in this simulation, both the intra- and intermolecular potential energies fluctuate around the average values and no unphysical drifts take place, in contrast to the LSC-IVR simulation where an increase in the intermolecular potential energy of approximately 3.3 kcal/mol occurs during the initial 1 ps.[44] The preservation of the zero-point energy in our methodology is owing to the stable trajec-

tories in the extended phase space including the WP width variables. The preservation has also been confirmed in the previous study with the SGWP model.[74]

APPENDIX D: RADIAL DISTRIBUTION FUNCTIONS

Here, we describe the quantum mechanical evaluation of the RDF with the SQ wave function [Eq. (2)] in a single-component system consisting of N identical particles for simplicity. Note that generalization to a multi-component system is straightforward. If the system is homogeneous, the spatial correlation between two particles is described by the quantum mechanical expectation value of the pair distribution function in the δ-function representation,

$$
\begin{aligned}
g(\mathbf{x}) &= \frac{1}{Nd} \left\langle \sum_{j \neq k} \delta(\mathbf{x} - (\mathbf{q}_j - \mathbf{q}_k)) \right\rangle \\
&= \frac{1}{Nd} \frac{1}{(\sqrt{2\pi})^3} \sum_{j \neq k} \{\det(\mathbf{B}_{jk})\}^{-1/2} \\
&\quad \times \exp\left[-\frac{1}{2}(\mathbf{x} - \mathbf{r}_{jk})^{\mathrm{T}} \mathbf{B}_{jk}^{-1} (\mathbf{x} - \mathbf{r}_{jk}) \right], \quad \text{(D1)}
\end{aligned}
$$

where d denotes the number density of the system, and the 3 × 3 real symmetric matrix $\mathbf{B}_{jk}$ is given in Eq. (A4). Finally, if the system is also spatially isotropic, the pair distribution function in Eq. (D1) can be reduced to the RDF which depends only on the magnitude $|\mathbf{x}|$.
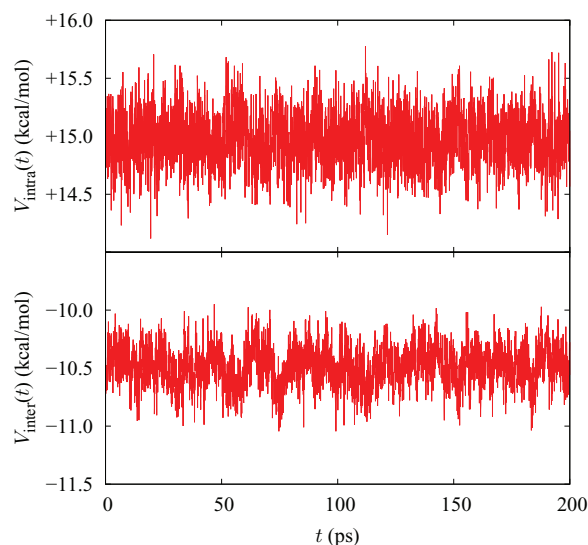

FIG. 9. Time development of the intra- and intermolecular potential energies obtained from the EGWP model. The average values (the SDs) of the intra- and intermolecular potential energies are 15.0 (0.23) and -10.5 (0.17) kcal/mol, respectively.

[1] D. Eisenberg and W. Kauzmann, *The Structures and Properties of Water* (Oxford University Press, New York, 1969).
[2] *Water: A Comprehensive Treatise*, edited by F. Franks (Plenum, New York, 1972), Vols. 1–7.
[3] G. W. Robinson, S.-B. Zhu, S. Singh, and M. W. Evans, *Water in Biology, Chemistry and Physics* (World Scientific, Singapore, 1996).
[4] I. Ohmine and H. Tanaka, Chem. Rev. **93**, 2545 (1993).
[5] I. Ohmine and S. Saito, Acc. Chem. Res. **32**, 741 (1999).
[6] R. Rey, K. B. Møller, and J. T. Hynes, Chem. Rev. **104**, 1915 (2004).
[7] P. Ball, Chem. Rev. **108**, 74 (2008).
[8] H. J. Bakker and J. L. Skinner, Chem. Rev. **110**, 1498 (2010).
[9] D. Laage and J. T. Hynes, Science **311**, 832 (2006).
[10] D. Laage and J. T. Hynes, J. Phys. Chem. B **112**, 14230 (2008).
[11] D. Laage, G. Stirnemann, F. Sterpone, R. Rey, and J. T. Hynes, Annu. Rev. Phys. Chem. **62**, 395 (2011).
[12] D. Laage, G. Stirnemann, F. Sterpone, and J. T. Hynes, Acc. Chem. Res. **45**, 53 (2012).
[13] M. Ji, M. Odelius, and K. J. Gaffney, Science **328**, 1003 (2010).
[14] R. T. Hart, C. J. Benmore, J. Neuefeind, S. Kohara, B. Tomberli, and P. A. Egelstaff, Phys. Rev. Lett. **94**, 047801 (2005).
[15] A. K. Soper and C. J. Benmore, Phys. Rev. Lett. **101**, 065502 (2008).
[16] C. Huang, K. T. Wikfeldt, T. Tokushima, D. Nordlund, Y. Harada, U. Bergmann, M. Niebuhr, T. M. Weiss, Y. Horikawa, M. Leetmaa, M. P. Ljungberg, O. Takahashi, A. Lenz, L. Ojamae, A. P. Lyubartsev, S. Shin, L. G. M. Pettersson, and A. Nilsson, Proc. Natl. Acad. Sci. U.S.A. **106**, 15214 (2009).
[17] A. Nilsson and L. G. M. Pettersson, Chem. Phys. **389**, 1 (2011).
[18] K. Nishizawa, N. Kurahashi, K. Sekiguchi, T. Mizuno, Y. Ogi, T. Horio, M. Oura, N. Kosugi, and T. Suzuki, Phys. Chem. Chem. Phys. **13**, 413 (2011).
[19] S. Ashihara, N. Huse, A. Espagne, E. T. J. Nibbering, and T. Elsaesser, J. Phys. Chem. A **111**, 743 (2007).
[20] R. Rey, F. Ingrosso, T. Elsaesser, and J. T. Hynes, J. Phys. Chem. A **113**, 8949 (2009).
[21] T. Yagasaki, J. Ono, and S. Saito, J. Chem. Phys. **131**, 164511 (2009).
[22] T. Yagasaki and S. Saito, Acc. Chem. Res. **42**, 1250 (2009).
[23] P. Hamm and J. Savolainen, J. Chem. Phys. **136**, 094516 (2012).

[24] P. Hamm, J. Savolainen, J. Ono, and Y. Tanimura, J. Chem. Phys. **136**, 236101 (2012).

[25] G. Jancso and W. A. Van Hook, Chem. Rev. **74**, 689 (1974).

[26] R. A. Kuharski and P. J. Rossky, J. Chem. Phys. **82**, 5164 (1985).

[27] H. A. Stern and B. J. Berne, J. Chem. Phys. **115**, 7622 (2001).

[28] M. Shiga, M. Tachikawa, and S. Miura, J. Chem. Phys. **115**, 9149 (2001).

[29] B. Chen, I. Ivanov, M. L. Klein, and M. Parrinello, Phys. Rev. Lett. **91**, 215503 (2003).

[30] X.-Z. Li, B. Walker, and A. Michaelides, Proc. Natl. Acad. Sci. U.S.A. **108**, 6369 (2011).

[31] T. E. Markland and B. J. Berne, Proc. Natl. Acad. Sci. U.S.A. **109**, 7988 (2012).

[32] B. Pamuk, J. M. Soler, R. Ramírez, C. P. Herrero, P. W. Stephens, P. B. Allen, and M.-V. Fernández-Serra, Phys. Rev. Lett. **108**, 193003 (2012).

[33] M. E. Tuckerman, *Statistical Mechanics: Theory and Molecular Simulation* (Oxford University Press, New York, 2010).

[34] N. Makri, Annu. Rev. Phys. Chem. **50**, 167 (1999).

[35] Y. Tanimura, J. Phys. Soc. Jpn. **75**, 082001 (2006).

[36] T. Schlick, *Molecular Modeling and Simulation: An Interdisciplinary Guide*, 2nd ed. (Springer, New York, 2010).

[37] G. A. Voth, Adv. Chem. Phys. **93**, 135 (1996).

[38] F. Paesani, S. Iuchi, and G. A. Voth, J. Chem. Phys. **127**, 074506 (2007).

[39] F. Paesani and G. A. Voth, J. Phys. Chem. B **113**, 5702 (2009).

[40] F. Paesani, S. Yoo, H. J. Bakker, and S. S. Xantheas, J. Phys. Chem. Lett. **1**, 2316 (2010).

[41] I. R. Craig and D. E. Manolopoulos, J. Chem. Phys. **121**, 3368 (2004).

[42] T. F. Miller III and D. E. Manolopoulos, J. Chem. Phys. **123**, 154504 (2005).

[43] S. Habershon, T. E. Markland, and D. E. Manolopoulos, J. Chem. Phys. **131**, 024501 (2009).

[44] S. Habershon and D. E. Manolopoulos, J. Chem. Phys. **131**, 244518 (2009).

[45] W. H. Miller, J. Phys. Chem. A **105**, 2942 (2001).

[46] J. Liu, W. H. Miller, F. Paesani, W. Zhang, and D. A. Case, J. Chem. Phys. **131**, 164509 (2009).

[47] J. Liu, W. H. Miller, G. S. Fanourgakis, S. S. Xantheas, S. Imoto, and S. Saito, J. Chem. Phys. **135**, 244503 (2011).

[48] E. J. Heller, J. Chem. Phys. **62**, 1544 (1975).

[49] E. J. Heller, J. Chem. Phys. **64**, 63 (1976).

[50] E. Kluk, M. F. Herman, and H. L. Davis, J. Chem. Phys. **84**, 326 (1986).

[51] S. Habershon, J. Chem. Phys. **136**, 014109 (2012).

[52] N. Corbin and K. Singer, Mol. Phys. **46**, 671 (1982).

[53] R. D. Coalson and M. Karplus, J. Chem. Phys. **93**, 3919 (1990).

[54] V. Buch, J. Chem. Phys. **117**, 4738 (2002).

[55] I. Burghardt, H.-D. Meyer, and L. S. Cederbaum, J. Chem. Phys. **111**, 2927 (1999).

[56] I. Burghardt, M. Nest, and G. A. Worth, J. Chem. Phys. **119**, 5364 (2003).

[57] I. Burghardt, K. Giri, and G. A. Worth, J. Chem. Phys. **129**, 174104 (2008).

[58] H. Wang and M. Thoss, J. Chem. Phys. **119**, 1289 (2003).

[59] P. A. Frantsuzov and V. A. Mandelshtam, J. Chem. Phys. **121**, 9247 (2004).

[60] H. Cartarius and E. Pollak, J. Chem. Phys. **134**, 044107 (2011).

[61] E. Hairer, C. Lubich, and G. Wanner, *Geometric Numerical Integration* (Springer-Verlag, Berlin, 2002).

[62] B. Leimkuhler and S. Reich, *Simulating Hamiltonian Dynamics* (Cambridge University Press, New York, 2005).

[63] R. Jackiw and A. Kerman, Phys. Lett. **71**, 158 (1979).

[64] P. Kramer and M. Saraceno, *Geometry of the Time-Dependent Variational Principle in Quantum Mechanics* (Springer, Berlin, 1981).

[65] K. G. Kay, Phys. Rev. A **46**, 1213 (1992).

[66] D. V. Shalashilin and I. Burghardt, J. Chem. Phys. **129**, 084104 (2008).

[67] F. Arickx, J. Broeckhove, E. Kesteloot, L. Lathouwers, and P. van Leuven, Chem. Phys. Lett. **128**, 310 (1986).

[68] F. Cooper, S. Y. Pi, and P. N. Stancioff, Phys. Rev. D **34**, 3831 (1986).

[69] Y. Tsue, Prog. Theor. Phys. **88**, 911 (1992).

[70] A. K. Pattanayak and W. C. Schieve, Phys. Rev. E **50**, 3601 (1994).

[71] D. Klakow, C. Toepffer, and P. G. Reinhard, J. Chem. Phys. **101**, 10766 (1994).

[72] K. Ando, J. Chem. Phys. **121**, 7136 (2004).

[73] K. Ando, J. Chem. Phys. **125**, 014104 (2006).

[74] K. Hyeon-Deuk and K. Ando, J. Chem. Phys. **131**, 064501 (2009).

[75] K. Hyeon-Deuk and K. Ando, J. Chem. Phys. **132**, 164507 (2010).

[76] J. Ono, K. Hyeon-Deuk, and K. Ando, "Semiquantal molecular dynamics simulations of hydrogen-bond dynamics in liquid water using spherical gaussian wave packets," Int. J. Quantum Chem. (in press).

[77] O. V. Prezhdo and Y. V. Pereverzev, J. Chem. Phys. **113**, 6557 (2000).

[78] O. V. Prezhdo, J. Chem. Phys. **117**, 2995 (2002).

[79] O. V. Prezhdo, Theor. Chem. Acc. **116**, 206 (2006).

[80] E. Heatwole and O. V. Prezhdo, J. Chem. Phys. **126**, 204108 (2007).

[81] Y. Shigeta, H. Miyachi, and K. Hirao, J. Chem. Phys. **125**, 244102 (2006).

[82] Y. Shigeta, Bull. Chem. Soc. Jpn. **82**, 1323 (2009).

[83] Y. Shigeta, H. Miyachi, T. Matsui, N. Yokoyama, and K. Hirao, in *Advances in the Theory of Atomic and Molecular Systems*, Progress in Theoretical Chemistry and Physics Vol. 20, edited by P. Piecuch, J. Maruani, G. Delgado-Barrio, and S. Wilson (Springer, 2009), pp. 3–34.

[84] Y. Shigeta, T. Inui, T. Baba, K. Okuno, H. Kuwabara, R. Kishi, and M. Nakano, "Quantal cumulant mechanics and dynamics for multidimensional quantum many-body clusters," Int. J. Quantum Chem. (in press).

[85] K. Ando, Bull. Chem. Soc. Jpn. **82**, 975 (2009).

[86] K. Ando, Chem. Phys. Lett. **523**, 134 (2012).

[87] K. Hyeon-Deuk and K. Ando, Chem. Phys. Lett. **532**, 124 (2012).

[88] J. Kucar, H. D. Meyer, and L. S. Cederbaum, Chem. Phys. Lett. **140**, 525 (1987).

[89] See, for example, Appendix of Ref. 70 and references therein.

[90] H. Yoshida, Phys. Lett. A **150**, 262 (1990).

[91] S. Nosé, J. Phys. Soc. Jpn. **70**, 75 (2001).

[92] T. F. Miller, M. Eleftheriou, P. Pattnaik, A. Ndirango, D. Newns, and G. J. Martyna, J. Chem. Phys. **116**, 8649 (2002).

[93] H. Okumura, S. G. Itoh, and Y. Okamoto, J. Chem. Phys. **126**, 084103 (2007).

[94] M. Tuckerman, B. J. Berne, and G. J. Martyna, J. Chem. Phys. **97**, 1990 (1992).

[95] H. Goldstein, C. Poole, and J. Safko, *Classical Mechanics*, 3rd ed. (Addison-Wesley, San Francisco, 2002).

[96] J. Ono, "A Theoretical Study of Hydrogen-Bond Dynamics in Liquid Water," Ph.D. dissertation, Kyoto University, 2012.

[97] In the present derivation, we neglect the degeneracy of eigenvalues for simplicity; for more detailed discussion on the degeneracy, see Appendix of Ref. 53.

[98] This is due to the practical complexity of quantizing the potential functions in the f-SPC model described in Sec. IV B in the case of the single-molecule (or intermediate) approximation; in particular, the intramolecular cross term, V_{cross} in Eq. (54), which is difficult to express in terms of Gaussian functions yields the significantly complicated fourth-order expansion in the Taylor series [Eq. (26)]. In this regard, it can be more practical to develop new model potentials designed to fit well with the intramolecular quantization procedure. This shall be, however, left for future work.

[99] L. Dang and B. Pettitt, J. Phys. Chem. **91**, 3349 (1987).

[100] F. Paesani, W. Zhang, D. A. Case, T. E. Cheatham III, and G. A. Voth, J. Chem. Phys. **125**, 184507 (2006).

[101] Note that the SPC/Fd model has one additional harmonic term for the H–H bond (i.e., the Urey-Bradley term). In this regard, Hyeon-Deuk and Ando state "The Urey-Bradley term adds effective anharmonicity to the potential and ..." (see Ref. 74). However, we found that the Urey-Bradley term mainly introduces the linear coupling between the O–H bond length and the H–O–H angle, and the anharmonicity of the O–H bond length is indeed negligible (for detailed discussion, see Ref. 96).

[102] K. Toukan and A. Rahman, Phys. Rev. B **31**, 2643 (1985).

[103] In some flexible models (e.g., the SPC/Fd, q-SPC/Fw, and q-TIP4P/F models), the intramolecular bending potential function consists of the quadratic form in the H–O–H angle, which is in general difficult to quantize in the SQGWP theory. In our previous studies reported in Refs. 74–76, the Taylor series of the bending potential in the Cartesian coordinates is indeed truncated at the second-order since the fourth-order expansion is too complicated to derive and implement. In the present theory, however, it is found that the second-order truncation results in numerically unstable trajectories due to the anisotropic delocalization of the EGWPs, and for this reason we have chosen the different water model which does not include the angle variables, instead of implementing the fourth-order expansion of the angular function. Another reason for not employing the q-TIP4P/F model is the presence of the negative charge on the M-point placed near the oxygen atom along the bisector of the H–O–H angle, which makes the fourth-order expansion of the intermolecular Coulomb potential more complicated than that of the typical three-site water models.

[104]Note that in the original model suggested in Ref. 102, the anharmonic O–H interaction has been expressed in terms of the Morse potential, but instead the quartic potential was utilized in the current study to avoid the dissociation of the O–H covalent bond, as in the case of the q-TIP4P/F model.

[105]T. E. Markland and D. E. Manolopoulos, J. Chem. Phys. **129**, 024105 (2008).

[106]K. Ando, J. Phys. Chem. B **112**, 250 (2008).

[107]S. Bubin and L. Adamowicz, J. Chem. Phys. **124**, 224317 (2006).

[108]G. Hura, D. Russo, R. M. Glaeser, T. Head-Gordon, M. Krack, and M. Parrinello, Phys. Chem. Chem. Phys. **5**, 1981 (2003).

[109]A. K. Soper, J. Phys.: Condens. Matter **19**, 335206 (2007).

[110]K. T. Wikfeldt, M. Leetmaa, M. P. Ljungberg, A. Nilsson, and L. G. M. Pettersson, J. Phys. Chem. B **113**, 6246 (2009).

[111]Note that the first intermolecular peak and subsequent first minimum of the O–H RDF obtained from the RMC method have non-negligible uncertainties arising from different H-bond constraints imposed in the fitting processes although all the structure models show an equally good fit to the diffraction experiments in reciprocal space (for details see Ref. 110), and thus the quantitative comparison of the O–H RDFs in this radial region in real space is difficult at present.

[112]C. J. Burnham and S. S. Xantheas, J. Chem. Phys. **116**, 1479 (2002).

[113]The statistical averages of the WP widths for the hydrogen atom along the x-, y-, and z-axes are 0.08, 0.14, and 0.18 Å, respectively; here, the WP widths are calculated from square roots of the diagonal elements of the WP width matrix in the body-fixed frame.

[114]The weaker intermolecular interactions at the intermediate state lead to the shorter O^*H^* bond length and the larger HO^*H^* bond angle, and simultaneously result in the WP localization along the x-axis and the WP delocalization along the y-axis.

[115]R. Kumar, J. R. Schmidt, and J. L. Skinner, J. Chem. Phys. **126**, 204107 (2007).

[116]J. A. Poulsen, G. Nyman, and P. J. Rossky, J. Phys. Chem. B **108**, 19799 (2004).

[117]T. F. Miller III and D. E. Manolopoulos, J. Chem. Phys. **122**, 184503 (2005).

[118]T. D. Hone, P. J. Rossky, and G. A. Voth, J. Chem. Phys. **124**, 154103 (2006).

[119]A. Nakayama and N. Makri, J. Chem. Phys. **125**, 024503 (2006).

[120]J. Liu and W. H. Miller, J. Chem. Phys. **127**, 114506 (2007).

[121]K. Kim and S. Saito, J. Chem. Phys. **133**, 044511 (2010).

[122]Y. Nagata and S. Mukamel, J. Am. Chem. Soc. **133**, 3276 (2011).

[123]M. A. Berg, Adv. Chem. Phys. **150**, 1 (2012).